



Review

Design and architecture of metal organic frameworks for visible light enhanced hydrogen production



Meicheng Wen^a, Kohsuke Mori^{a,b,c,*}, Yasutaka Kuwahara^{a,b}, Taicheng An^d,
Hiromi Yamashita^{a,b,*}

^a 1-2 Yamadaoka, Graduate School of Engineering, Osaka University, Osaka, 565-0871, Japan

^b Unit of Elements Strategy Initiative for Catalysts & Batteries, Kyoto University, ESICB, Kyoto University, Japan

^c JST, PRESTO, 4-1-8 Honcho, Kawaguchi, Saitama, 332-0012, Japan

^d Guangzhou Key Laboratory of Environmental Catalysis and Pollution Control, School of Environmental Science and Engineering, Institute of Environmental Health and Pollution Control, Guangdong University of Technology, Guangzhou, 510006, China

ARTICLE INFO

Article history:

Received 1 May 2017

Received in revised form 23 June 2017

Accepted 26 June 2017

Available online 27 June 2017

Keywords:

Metal organic frameworks

Hydrogen production

Visible light enhanced

Organometallic compounds

Dye-sensitized

ABSTRACT

MOFs offers a potential platform for anchoring photosensitizers and catalytic moieties, encapsulating metal nanoparticles, and supporting the semiconductor to drive chemical H₂ production reactions by taking the advantages of large surface area, permanent pores and tunable channels as well as tailorable physical and chemical functions. Recently, considerable attention has been paid to the application of MOFs in heterogeneous photocatalysis for H₂ production. In this review, the latest progress of MOFs involved in the reaction of H₂ production from water and visible-light-enhanced H₂ releasing from hydrogen carriers were summarized. The successful methods to maximize photocatalytic activity of H₂ production from water by introducing light sensitization and anchoring catalytic sites within MOFs, tuning the band gap of MOFs by modification of functional groups were also highlighted. Also the latest advances in heterogeneous organic dye-sensitized metal nanoparticle supported on MOFs for photocatalytic H₂ production and visible light enhanced H₂ production from H₂ carriers were emphasize. In the end, a brief perspective to the challenges and new development directions in the development of highly active MOFs to achieve high photocatalytic activity in the H₂ production is also discussed, which would be of great interest in the solar energy conversion.

© 2017 Elsevier B.V. All rights reserved.

Contents

1. Introduction	556
2. Semiconducting behavior of MOFs	557
3. Photocatalytic H ₂ production from water driven by MOFs	557
4. Organometallic compounds functionalized MOFs for photocatalytic H ₂ production from water	559
5. Semiconductor/MOFs photocatalysts-driven photocatalytic H ₂ production from water	562
6. Dye-sensitized MOFs-involved H ₂ production system	563
7. MOF templated nanocomposite for photocatalytic H ₂ production from water	566
8. Metal nanoparticle loaded MOFs for visible light enhanced H ₂ production from hydrogen storage materials	566
8. Summary and outlook	567
Acknowledgements	568
References	568

* Corresponding authors at: 1-2 Yamadaoka, Graduate School of Engineering, Osaka University, Osaka, 565-0871, Japan.

E-mail addresses: mori@mat.eng.osaka-u.ac.jp (K. Mori), yamashita@mat.eng.osaka-u.ac.jp (H. Yamashita).

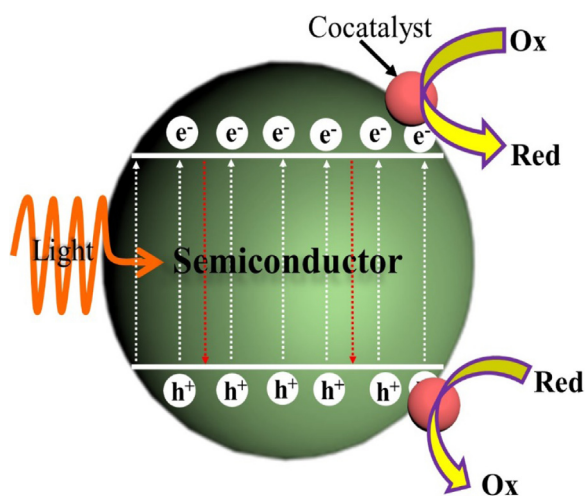


Fig. 1. Schematic illustration of photocatalytic reaction taking place on a semiconductor photocatalyst mediated by suitable redox cocatalysts.

1. Introduction

The worldwide problem of energy crises and environmental problem caused by the increasing use of the limited fossil fuels have received tremendous researcher's attention in the search for clean and renewable energy sources [1,2]. In fact solar energy is an inexhaustible natural resource. The magnitude of available solar energy striking on the surface of the earth (1.3×10^5 TW), which is much larger than the energy consumed by humanity per year (1.6×10^1 TW in 2010) [3], is a highly appealing source of natural energy. The conversion of solar energy into chemical energy in the form of chemical bonds is considered as a highly desirable approach to fulfill the requirement of sustainable development. Inspired by the natural photosynthesis of green plants and some other microorganisms with efficient converting solar energy into chemical energy in the form of carbohydrates or hydrogen, the field of photocatalysis has expanded rapidly over the past several years and it is recognized as the most promising technology for converting solar energy into useful chemical potential for synthetic purposes [4–6]. Especially, semiconductor-based photocatalysis has received considerable attention because of its potential applications in energy exploitation [7] and environmental purification [8], since the discovery of the Honda-Fujishima effect on water splitting for H_2 production over TiO_2 photoelectrodes in 1972 [9]. Increasing efforts have been devoted to explore light responsive materials for visible light driven photocatalytic reaction [10].

The development of new environment-friendly, low-cost and highly stable materials has become one of the most urgent and challenging issues related to global energy crisis and pollution problem [11]. Semiconductor are considered as one of the most promising photocatalysts for various photoredox reactions, because of suitable band gap, low cost, high chemical stability, and environmental benign [12]. Fig. 1 displays the schematic illustration of photocatalytic reaction taking place on a semiconductor photocatalyst mediated by suitable redox cocatalysts. When the energy of incident light is higher than that of bandgap, electrons are generated through band-gap excitation and transferred from the valence band to conductive band of photocatalyst particles, leaving the holes in the valence band. The photo-generated electrons may go through the following possible pathways: (1) transferred to surface active sites and subsequently involved in surface redox reaction, where the hole is involved in photocatalytic oxidation reaction; (2) captured by the defect sites in the bulk of semiconductors;

(3) recombine with photo-generated holes by releasing the excess energy to the surrounding environment.

Considering that the chemical reactions usually occur on the surface of photocatalysts, the redox reactions of adsorbed species with photoexcited electron-hole pairs and the recombination of photoexcited electron-hole pairs are two competing processes. The first pathway is favored, where the second and third pathway are not desirable. Therefore, reducing the recombination rate of photoexcited electron-hole pairs is the critical way to enhance the photocatalytic performance. On the other hand, solar light contains less than 5% of ultraviolet (UV) light, about 42–43% visible light (400–700 nm) [13], and 52–55% infrared (>700 nm). In the consideration of efficient utilization of visible light, the development of a photocatalyst with a wide range of visible light absorption is indispensable. However, most of the reported photocatalysts are only responsive to UV light [14]. To this end, numerous attempts have been made to promote the transformation of photo-excited electron-hole pairs from bulk to the surface of semiconductor and synthesis of visible light responsive semiconductor by various techniques, such as doping semiconductor with metal or nonmetal elements [15–18], morphology controlling [19,20], size turning [21], loading with plasmonic nanoparticles (such as gold, silver and copper) [22–24], forming heterojunction by coupling with narrow-band-gap semiconductors [25], or atomic structure engineering [26]. Apart from this, various types of visible light responsive semiconductors have also been explored and studied for artificial photosynthesis [27–29]. Even though recent intensive efforts and exciting achievements in the H_2 production from water have been done [30], the development of visible light driven photocatalysts with narrow band gap that can efficiently utilize entire solar spectrum to driven H_2 production with high catalytic activity and stability is still a challenge for the research community.

Metal-organic frameworks (MOFs) are constructed from inorganic metal ions as connecting centers and organic moieties as linkers. Such inorganic-organic polymers offer significant chemical diversity because they can be modified by functional groups and, they have been widely employed in many applications such as catalysis, gas sorption, energy storage, and membrane [31,32]. MOFs have several advantages over other inorganic materials [33]. Firstly, photoactive organic linker endows the MOFs semiconducting properties. Upon light irradiation, the organic linker acts as an antenna to capture light, electrons get excited from HOMO to LUMO state of organic linker, the photo-excited electrons further relay to nodes of MOFs through a linker-to-cluster charge-transfer mechanism (LCCT) to activate the metal nodes, subsequently involved in a heterogeneous photoredox reaction, such as CO_2 reduction, water splitting, degradation of organic pollutants, or organosynthesis [34,35]. Secondly, controllable physical and chemical properties, extraordinarily high surface area and a great number of functional groups can allow the efficient adsorption and diffusion of reactant and product molecules [36]. Furthermore, it is easy to tailor the chemical properties of MOFs and at the same time to enrich structural diversity in MOFs through synthetic modification [37], the linker of MOFs can be integrally or partially replaced by other organic linker via the mix-and-match synthetic strategy [38]. Moreover, the nodes of MOFs can also be replaced by foreign metal ions [39]. It is clear that MOFs provide a great opportunity for heterogeneous photocatalysis due to the richness of metal-containing center and organic bridging linker, as well as the controllability of the synthesis. In the last five years, MOFs have been extensively exploited as photocatalysts for H_2 production from water and have proved to be important alternatives to semiconductor photocatalysts and metal complexes photocatalysts. Tremendous efforts have been dedicated to design and architecture of visible-light-responsive MOFs for enhanced hydrogen production from water and the interest is continuously increasing. Thus, a review of the recent advances

and challenges of MOF-involved H_2 production system is of great importance.

In this review, the recent progress in the design and architecture of photoactive MOFs by using various novel techniques and their efficient application in photocatalytic H_2 generation were summarized and highlighted. Considering the present MOFs involved in heterogeneous photocatalytic H_2 production, the reviewing can be classified into following categories: (1) MOFs photocatalysts, including MOF functionalized with organometallic compound. In MOFs photocatalyst driven catalytic hydrogen generation reaction, MOFs act as sole photo- and catalytic active sites rather than support materials. The incident light are mainly absorbed by the linker of the MOFs, the photogenerated electrons from the linker of MOFs relay to nodes of MOFs and co-catalysts to drive the photocatalytic hydrogen production; (2) semiconductor/MOFs photocatalysts. In this hybrid systems, irradiated light is absorbed partly by the linkers of MOFs and mainly by semiconductors. MOFs acts as support and co-catalyst to allow effective dispersion of semiconductors, enhancing the solar light absorption, and promoting the kinetic processes of both charge separation and catalytic reactions; (3) dye-sensitized MOFs. In this system, dye molecular is used as a light absorbing antenna to harvest light, excited dye molecular generate electrons that subsequently transfer to the surface of MOFs and co-catalysts to induce a heterogeneous photoredox reaction. (4) MOF templated photocatalysts. In this case, MOF is used as sacrificial template to obtain novel photocatalysts nanocomposite and used it for H_2 production. In addition, visible light enhanced H_2 releasing from energy carriers over metal nanoparticle supported MOF were also summarized. Owing to the bright future of those photoactive metal organic frameworks in photocatalysis for environment cleaning and energy production, we sincerely hope those powerful materials can serve as eco-materials to replace commercially available photocatalysts for practical application. In the end, a short perspective on the challenges and new directions in the development of highly active MOFs to achieve high photocatalytic activity of H_2 production is also discussed, which would be of great interest in the solar energy conversion.

2. Semiconducting behavior of MOFs

The semiconducting property of MOFs is a prerequisite for photocatalytic H_2 production. The ways of characterizing the semiconducting behavior of MOFs were summarized here, offering the methods to recognize whether MOF has semiconducting properties. The direct evidence to confirm the semiconducting behavior of MOFs is the electron conductivity. Kobayashi and his co-workers [40] reported the synthesis of $Cu[Ni(pdt)_2]$ with a band gap about 2 eV, and the electrical conductivity of this compound was measured to be $1 \times 10^{-8} \text{ S cm}^{-1}$ which is lower than the conductivity of metal (10^1 to 10^5 S cm^{-1}) but higher than the insulator (below $10^{-10} \text{ S cm}^{-1}$), suggesting $Cu[Ni(pdt)_2]$ is a semiconductor. Moreover, the electrical conductivity can be dramatically improved under a stream of I_2 vapor treatment at 50°C by 10^4 -fold, indicating the *p*-type semiconducting properties of $Cu[Ni(pdt)_2]$. When the MOFs are participating in the photocatalytic reaction, the mobility of electrons and holes of MOFs is more important than the electrical conductivity in achieving high activity. Gascon et al. [41] reported that the charges mobility of MIL-125(Ti) is about $10^{-5} \text{ cm}^2 \text{ V}^{-1} \text{ s}^{-1}$ upon 340 nm light illumination, and a significant decrease was observed upon lowering the temperature to 153 K, indicating that the thermally activated hopping is the main mechanism for the charge transport due to the organic linker isolated Ti clusters.

An early work of three novel MOFs $[Co_2(C_{10}H_8N_2)] [C_{12}H_8O(COO)_2]_2$, $[Ni_2(C_{10}H_8N_2)] [C_{12}H_8O(COO)_2]_2 \cdot H_2O$, and $[Zn_2(C_{10}H_8N_2)] [C_{12}H_8O(COO)_2]_2$ with three

dimensional structures involved in photocatalytic reaction was reported by Mahata et al. in 2006 [42]. All the compounds displayed photocatalytic activity for the degradation of organic dyes (orange G, rhodamine B, Remazol Brilliant Blue R, and methylene blue). The mechanism for photocatalytic degradation of organic dyes was explained as following: the photo-excited electron transfer from the HOMO state to LUMO state of linker upon UV light irradiation. Unstable HOMO state received one electron from organic dye to return to its ground state accompanied by destroying organic dye molecular structure, where the excited electron in the LUMO state captured by the O_2 dissolved in solution to form superoxide anion and subsequently involved in the degradation of dye molecular. Inspired by this work, MOF-5 in a formula of $Zn_4O(BDC)_3 \cdot (DMF)_8(C_6H_5Cl)$, (BDC: 1,4-benzenedicarboxylate, DMF: N,N-Dimethylformamide) was designed and synthesized by Yaghi and his co-workers in 1999 [43]. Alvaro et al. [44] also demonstrated that MOF-5 is a microporous semiconductor enabling the production of photoactive charges upon light excitation, which undergoes charge separation decaying in the microsecond time scale. The conduction band energy of MOF-5 is calculated to be 0.2 V versus NHE with a band gap of 3.4 eV. The photocatalytic degradation of phenol in aqueous solution was used as a probe to confirm the semiconducting behavior of MOF-5. This compound exhibited remarkable photocatalytic activity for the degradation of phenol. Additionally, based on density functional theory calculations, the band gap of MOF-5 can be engineered by substitution of foreign metal ions (Zn, Cd, Be, Mg, Ca, Sr Ba) and anion atoms (S, Se, Te) in the nodes of MOF-5 from 3.6 to 1.7 eV [45]. Another methodology to modify the band gap of MOF is rational functionalization of the linking unit. The band gap of MIL-125(Ti) can be systematically engineered by changing the ratio between BDC, NH_2 -BDC, and $(NH_2)_2$ -BDC [46]. Up to now, several representative MOF photocatalysts have been investigated in environmental and energy science [47]. On the basis of above experimental and theoretical analysis, it is now clear that the optical properties and band gaps of MOFs can be systemically modified, holding great potentials for photocatalytic H_2 production. However, a small number of MOFs were proven to be effective for photocatalytic H_2 production from water, and the activity of so far reported MOFs is very low. It is obvious that not only tuning the optical property and band gap modification, but also the active site engineering and photosensitizer immobilization, discussed below, is the critical way to improve catalytic activity.

3. Photocatalytic H_2 production from water driven by MOFs

Water splitting, in which the solar light is used to break down H_2O to produce H_2 and O_2 over photocatalysts, is of significant importance to convert and store solar energy as chemical fuels in a sustainable manner [3]. The most studied photocatalyst for photocatalytic water splitting is semiconductor. After absorption of visible light by semiconductor, electrons are excited and transfer to the conduction band (CB) and holes are left in the valence band (VB). The photoexcited electron reacts with proton to produce hydrogen, while holes react with reductive reactant to form oxidative products. MOFs undergoes a similar reaction process, and the energy levels are typically characterized by the highest occupied molecular orbital (HOMO) and the lowest unoccupied molecular orbital (LUMO).

Fig. 2 illustrates photocatalytic H_2 production over photo-active MOFs. The organic linker can be considered as light absorption units to use the energy of solar light to generate electron and holes (Pathway 1). Most of inorganic clusters in MOFs are transition metal oxides (M_xO_y). These metal oxides are consisted of transition metal ions coordinated to the oxygen of organic linkers. The photo-

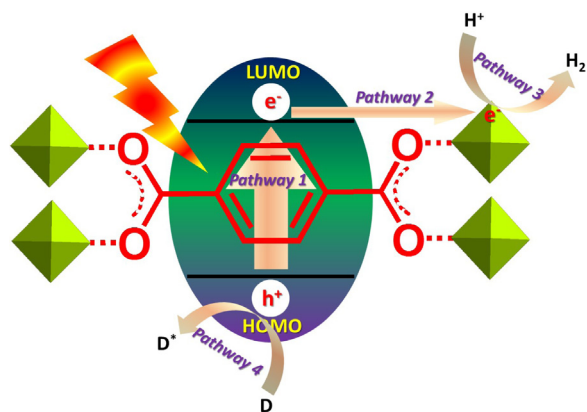


Fig. 2. Schematic illustration of photocatalytic water splitting over semiconducting MOFs; (Pathway 1) light harvesting by an organic linker; (Pathway 2) the electron transportation pathway; (Pathway 3) reaction of proton with electron to produce hydrogen over the inorganic cluster of MOFs; (Pathway 4) quenching of h^+ by a donor. (Inset) Basic components of MOFs: inorganic cluster and organic linker of MOFs, these components can be varied and modified to tailor physical and chemical properties of the resulting MOFs.

excited electron can transfer to the cluster of MOFs (Pathway 2) through a linker-to-cluster charge-transfer mechanism (LCCT). This LCCT mechanism have been confirmed by Li et al. [48], in which a photochromic test over $\text{NH}_2\text{-MIL-125 (Ti)}$ was carried out. The color of $\text{NH}_2\text{-MIL-125 (Ti)}$ suspension change from original bright yellow to green upon the visible light irradiation, and then the green color gradually turned back to its original bright yellow by bubbling CO_2 or O_2 gas under dark condition. The electron spin resonance (EPR) result indicated that Ti^{3+} formed in the cluster of MOFs under visible light irradiation. No Ti^{3+} signal was detected in bright yellow colored samples, evidenced that the electron transferred to the cluster of MOFs to reduce Ti(IV) to Ti(III) while light irradiating on MOFs. The proton which gathered around the cluster reacts with photoexcited electron to produce H_2 (Pathway 3). Meanwhile, the hole in the HOMO state of linker comes back to its ground state by accepting an electron from an electron donor (Pathway 4). It is well known that only the MOFs with LUMO state more negative than $\text{H}_2\text{O}/\text{H}_2$ couple (0.00 eV) are capable to drive the photocatalytic H_2 production from water under light irradiation. Up to now, only a handful of MOFs have been represented as photocatalysts for photocatalytic H_2 production from water upon the LCCT mechanism.

The first example of photoactive MOF $[\text{Ru}_2(p\text{-BDC})_2]_n$ ($p\text{-BDC}$ = 1,4-benzenedicarboxylate) for photocatalytic reduction of water into H_2 was reported by Mori and his co-workers in 2009 [49]. $[\text{Ru}_2(p\text{-BDC})_2]_n$ was constructed by linking the Ru_2 paddle-wheel motif with 1,4-benzenedicarboxylate as shown in Fig. 3. The turnover number based on Ru-MOFs was 8.16 at certain reaction conditions. In 2010, Garcia and co-workers [50] demonstrated that two highly water-resistant Zr-containing MOFs constructed from terephthalate (UiO-66) and 2-amino-terephthalate [UiO-66(NH_2)] linkers, are capable to serve as photocatalysts for H_2 generation from methanol or water/methanol upon UV light irradiation. The XRD patterns of UiO-66 and UiO-66(NH_2) indicate that the modification with amino group in UiO-66 does not change the crystal structure of the MOF, but extend the light absorption of MOFs to the visible region (Fig. 3a). UiO-66(NH_2) showed better photocatalytic activity of H_2 production than the MOFs without $-\text{NH}_2$ functional groups, because of the introduction of NH_2 within MOFs can not only extend the light absorption of MOFs to visible light region but also promote the charge separation efficiency. Once co-catalysts platinum nanoparticle was loaded on the surface of MOFs with the aim to promote charge separation, the total amount H_2 evolved over Pt loaded MOFs was almost three times as compared with the

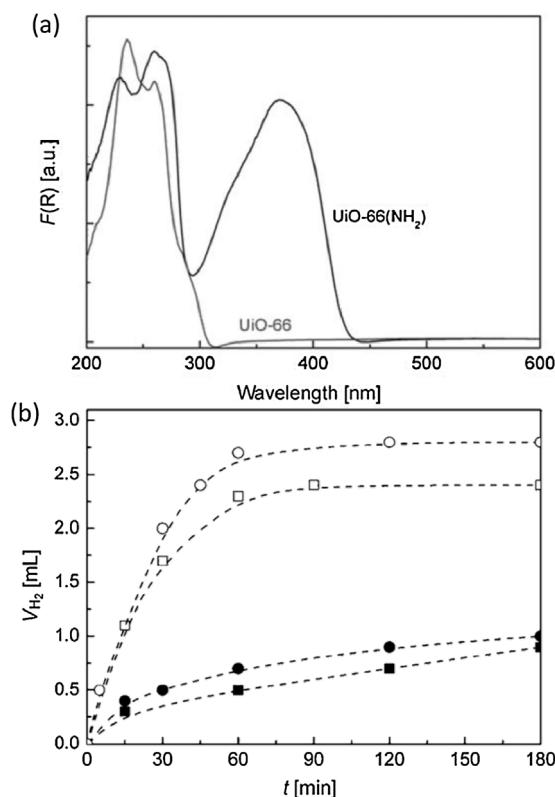


Fig. 3. (a) UV-vis spectra of UiO-66 and UiO-66(NH_2); (b) H_2 evolved during the photocatalytic reactions over UiO-66 (■), UiO-66 (NH_2) (●), UiO-66/Pt (□), and UiO-66(NH_2)/Pt (○) in water/methanol 3: 1 at UV light irradiation. Reproduced with permission from Ref. [50]. Copyright 2011 Wiley-VCH.

parental assemblies. The apparent quantum yield for H_2 evolution was 3.5% for UiO-66(NH_2) in a mixture of water and methanol (3: 1) by using monochromatic light of 370 nm. Although the apparent quantum yield still not very satisfactory, this study stimulated significant attention on exploiting MOFs as semiconductor participating in photocatalytic H_2 production from water.

Similar to the use of Ti incorporated porous material and carboxylate groups bridged titanium oxoclusters in the application of photocatalysis [51–53], Férey and co-workers [54] have developed highly porous titanium based MOFs (MIL-125(Ti)) using terephthalic acid to link titanium oxoclusters. The surface area of this crystallized MOF is up to $1550 \text{ m}^2 \text{ g}^{-1}$, which allows a large amount of alcohols adsorbed inside the MOF framework. Such UV light responsive MOF shows remarkable photocatalytic activity for the oxidation of alcohols. In order to attain efficient utilization of solar light, similar strategy for extending the absorption edge to visible light of UiO-66 by using amine-functionalized linker was explored. Horiuchi and co-workers [55] also reported a visible light responsive catalyst Ti-MOF- NH_2 for photocatalytic H_2 production from water. The MOFs was built from Ti titanium oxoclusters and 2-amino-benzenedicarboxylic acid. Ti-MOF- NH_2 exhibits a visible light absorption band extending to 500 nm which is associated with the chromophore in linking units. Photocatalytic H_2 production was performed under visible light irradiation by using triethanolamine (TEOA) as sacrificial electron donor and Pt nanoparticle as co-catalyst, respectively. Ti-MOF- NH_2 exhibits a slight photocatalytic activity, while about $3 \mu\text{mol}$ of H_2 was detected after 1 h visible light irradiation over Pt/Ti-MOF- NH_2 on the basis of LCCT mechanism, indicating that enhanced charge separation is caused by the inclusion of the platinum as co-catalyst. No photocatalytic H_2 production occurs on Pt/Ti-MOF without $-\text{NH}_2$ moiety, indicates that the visible-light absorption property of linkers are indispensable for

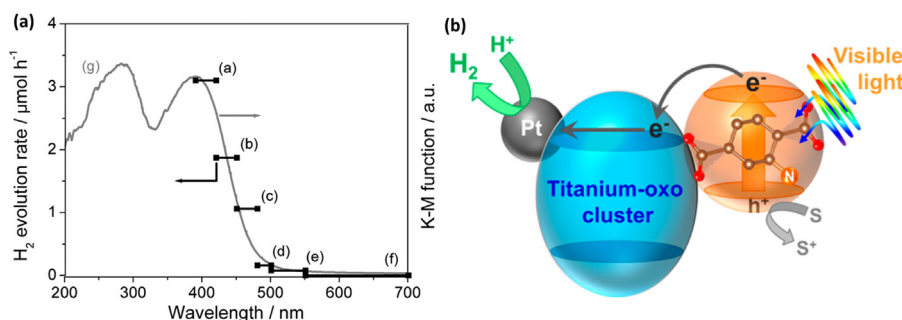


Fig. 4. (a) Wavelength-dependent H_2 evolution rate of Pt/Ti-MOF- NH_2 sample upon incident light irradiation ((a) 380–420 nm; (b) 420–450 nm; (c) 450–480 nm; (d) 480–500 nm; (e) 500–550 nm; (f) above 550 nm) and UV-vis absorption spectra (g) of Pt/Ti-MOF- NH_2 ; (b) Schematic illustration of photocatalytic hydrogen production reaction over Pt-supported Ti-MOF- NH_2 on the basis of the LCCT mechanism. Reproduced with permission from Ref. [55]. Copyright 2012 American Chemical Society.

achieving visible-light-driven photocatalytic H_2 production. The H_2 evolution rate of Pt/Ti-MOF- NH_2 was in line with the light absorption of linker as shown in Fig. 4a, suggesting that the amino-functionalization can efficiently absorb the incident visible light up to 500 nm to excite the electron from its HOMO state to LUMO state. The photo-excited electron transfer to the cluster of MOFs through LCCT mechanism as shown in Fig. 4b, resulting in reducing Ti^{4+} to Ti^{3+} . Signals associated with the characteristic of paramagnetic Ti^{3+} centers in a distorted rhombic oxygen ligand field were observed in EPR spectrum, suggesting the formation of Ti^{3+} [55].

The as-formed $\text{Ti}^{3+}/\text{Ti}^{4+}$ redox within MOFs can be further used to reduce oxidative metal salt precursors to fabricate highly dispersed metal nanoparticle (Au, Pd, and Pt) on Ti-MOF without using extra reducing and capping agents as reported by Wu's group [56]. The as-prepared Pt/Ti-MOF serve as efficient photocatalysts for H_2 production from water in the presence of triethanolamine as a sacrificial agent under UV light irradiation. The turnover number based on Pt was calculated to be 30.2, which is much higher than that of Pt/Ti-MOF prepared by a direct photo-deposition method.

In order to develop highly efficient, inexpensive noble-metal-free photocatalytic systems, enormous efforts have been devoted to broaden the light absorption region of photocatalysts by using the organic dye as photosensitizer and non-noble metal as co-catalysts to improve their photocatalytic performance [57,58]. MOFs offers a potential platform to integrate the organic dye with non-noble metal into a single framework. Zhang's [59] has synthesized a dye-like ligand-based MOFs (Gd-MOF), in which H_4abtc (3,3',5,5'-azobenzene tetracarboxylic acid) and Gd^{3+} were employed as linker and connecting center, respectively. Gd-MOF possesses excellent light-harvest property with absorption edge above 530 nm. The LUMO-HOMO gap of Gd-MOF was measured to be 2.35 eV. This porous material exhibits remarkable photocatalytic activity for H_2 generation by using TEOA as an electron donor under UV-vis irradiation, and the photocatalytic activity can be further enhanced by the deposition of Ag as co-catalyst. More recently, Zang's group [60] have developed a crystalline coordination polymer by using redox-active copper connected with rhodamine-derived ligand. Such Cu-based coordination polymer is highly active for the H_2 production from water, the highest H_2 production rate under optimized reaction condition is $7.88 \text{ mmol g}^{-1} \text{ h}^{-1}$ under visible light irradiation ($\lambda > 420 \text{ nm}$). These works open up new avenues for constructing MOFs photocatalysts using functional pigment groups as linker and active non-noble metal ions as connecting center to efficiently converting solar energy to chemical energy.

4. Organometallic compounds functionalized MOFs for photocatalytic H_2 production from water

Organometallic compounds are attractive catalysts for artificial photosynthesis [61]. Particularly, chemists have paid significant

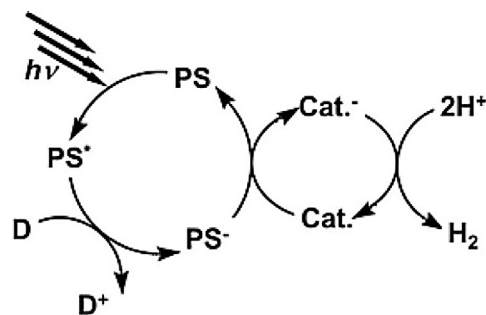


Fig. 5. A schematic illustration of a molecular based photocatalytic systems for proton reduction.

attention on developing organometallic dyes molecular based homogenous catalytic H_2 evolution systems [62]. Three fundamental components are needed to construct this H_2 evolution system as shown in Fig. 5: a photosensitizer (PS) to harvest sunlight for generating charge-separated excited states; a hydrogen generation catalyst (Cat.) to accept the photo-excited electron for catalyzing the reduction of proton to H_2 ; and a sacrificial agent (D) to recover the oxidative photosensitizer [63]. The overall reaction is considered as a visible-light-driven reduction of proton by a sacrificial reagent to molecular H_2 through electron relay. As so far, the H_2 production from water in homogeneous reaction with organometallic complexes have been well documented [64]. In spite of their outstanding achievement, the problems of harsh reaction conditions, poor selectivity, separation issues, and stability hinder their further application [65]. In this context, the integration of photosensitizer with catalyst components as covalent bonded dimers, coordination polymers, and supramolecular assemblies have attracted intensive attentions [66]. MOFs are assembled by the connection of secondary building blocks through rigid organic ligands. The most attractive feature of MOFs is their tunable property, which make MOF as an ideal platform to integrated photosensitizer with photocatalytic active site within a single solid to allow the absorption of solar energy to generated excited states by the photosensitizer part and transfer to catalytic active sites, where the reduction of proton takes place. Moreover, due to their high crystalline and porosity nature, the photo-generated charges transfer processes and pathway to the active site of MOF can be significantly accelerated and shorten. Therefore, the rational design of MOFs for incorporating both photosensitizer and active site in a single solid platform provides important insight into well organizing multiple components system for solar energy utilization.

A facile strategy that have been employed for metalation of MOFs is the using of the organic linker, which has donor site capable of chelating a metal ions. This method can be carried out by using an organic compound with two functional groups, one primary func-

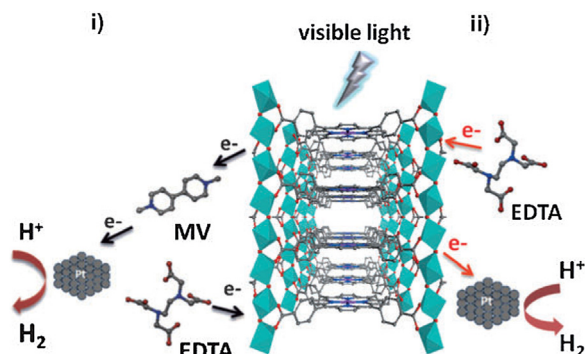


Fig. 6. Schematic illustration of photocatalytic H_2 production over ZnTCPP in the presence of methyl viologen (MV) (i) and in the absence of MV (ii). Reproduced with permission from Ref. [71]. Copyright 2012 Wiley-VCH.

tional group contributes to link the inorganic cluster to construct the framework, and the secondary functional group is employed to bind the extraneous metal ion but not involved in constructing MOFs. A prerequisite to apply this strategy relies upon that the secondary functional group is compatible with the MOFs synthesis, which means the growth process of MOFs does not affected by the secondary functional groups, thus allowing foreigner metal ions can coordinate with secondary functional group. A general way to realize this approach is the so-called mix-and-match synthetic strategy [67], in which the proportion of two different ligand building blocks with same length can be adjusted to obtain MOFs with same structural topology.

As porphyrins have been considered as versatile functional molecules and widely applied in catalyst and light harvesting [68,69], they have been employed as building blocks for constructing MOFs [70]. A guest-free base porphyrin within MOFs can serve as a free metal chelating site. One successful example of this technique was contributed by Rosseinsky's group [71] who employed porphyrins as functional organic ligands [free-base meso-tetra(4-carboxyl-phenyl) porphyrin (H_2TCPP)]. The reaction of $\text{AlCl}_3 \cdot 6\text{H}_2\text{O}$ with H_2TCPP in water under hydrothermal condition afford a water-stable porous porphyrin MOFs (Al-PMOF) with a high surface area up to $1400 \text{ m}^2 \text{ g}^{-1}$. There is no aluminium coordinated within the porphyrin ring after analyzing the composition of Al-PMOF. Subsequently, the metalation of Zn within the porphyrin ring was carried out in DMF solution containing zinc acetate. A highly crystalline purple sample $\text{Zn}_{0.986(12)}\text{TCPP}[\text{AlOH}]_2$ (here noted as ZnTCPP) with 90% of porphyrin center occupied by Zn was obtained. The photocatalytic properties of Al-PMOF and ZnTCPP was evaluated in a H_2 production system including Pt nanoparticle as co-catalyst, ethylenediamine tetraacetic acid (EDTA) as a sacrificial electron donor and methyl viologen as electron mediator. As shown in Fig. 6, the porphyrin rings of MOFs was reduced upon irradiating the suspension and consequent relay of an electron to reduce methyl viologen (MV) to $\text{MV}^{\bullet+}$ radical cation, while the positive porphyrin unit within the MOFs oxidized EDTA to organic decomposition products. $\text{MV}^{\bullet+}$ radical cation then give one electron to the colloidal Pt nanoparticle. Finally, the protons were reduced to H_2 on the Pt nanoparticles. However, due to the large size of methyl viologen, the mediation of an electron by MV was restricted by the small internal pore size of MOFs, resulting in the inefficient electron transfer from porphyrin to Pt nanoparticle. Therefore, only a small amount of H_2 was produced over Al-PMOF and ZnTCPP in the presence of MV. Once the MV was removed from the H_2 production system, the produced H_2 amount was significantly increased by more than one order of magnitude. In the case of without MV, the reduced porphyrin, generated by the reaction between photo-excited porphyrin molecules with EDTA, can directly transfers an

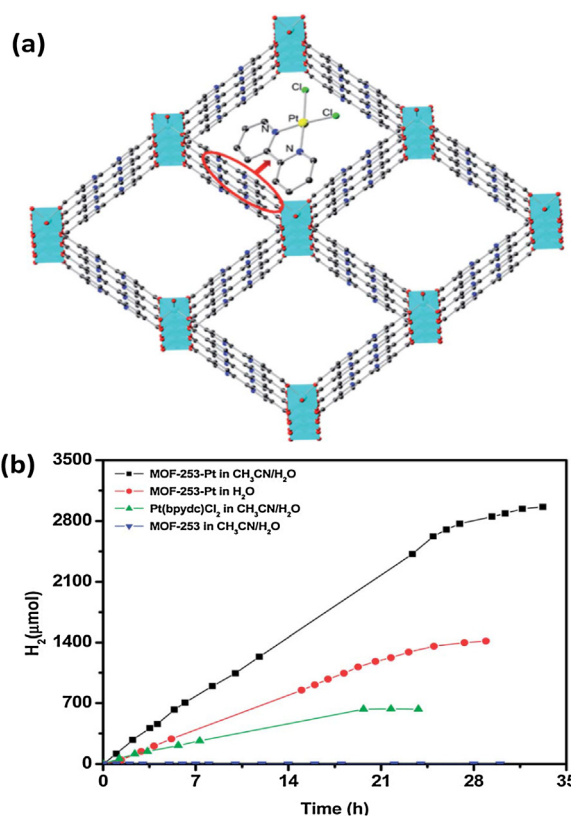


Fig. 7. (a) Model structure of MOF-253-Pt; (b) amount of H_2 evolved during the photocatalytic reaction using MOF-253-Pt (0.53 mM based on Pt), $\text{Pt}(\text{bpydc})\text{Cl}_2$ (0.53 mM based on Pt), and MOF-253 (1 equivalent MOF-253-Pt), respectively, reaction condition: 100 mL of $\text{CH}_3\text{CN}/\text{H}_2\text{O}$ (v/v, 1:1), 15% TEOA (v/v), pH = 8.5, visible light ($\lambda > 420 \text{ nm}$). Reproduced with permission from Ref. [77]. Copyright 2013 Royal Society of Chemistry.

electron to the Pt nanoparticle for H_2 production. The heterogeneous nature of photocatalytic H_2 production driven by MOFs was further confirmed by irradiating a supernatant solution with visible light. No H_2 could be detected, indicating the amount of H_2 is generated by heterogeneous reaction. Apart from the Zn ions can be anchored within the cavity of the porphyrin, but also Cu, and Fe ions were successfully incorporated into the metal free porphyrin rings without losing their high surface area and chemical stability [70,72].

Feng et al. [73] prepared a new biomimetic heterogeneous photocatalyst ($[\text{FeFe}]@\text{ZrPF}$) by immobilizing biomimetic $[\text{Fe}_2\text{S}_2]$ complexes ($[(\text{i-SCH}_2)_2\text{NC}(\text{O})\text{C}_5\text{H}_4\text{N}-\text{Fe}_2(\text{CO})_6]$) with a zirconium-porphyrin MOF(ZrPF). MOF(ZrPF) was constructed from a unit of tetrakis(4-carboxy-phenyl porphyrin)-zinc complex as linker and Zr ion as connecting center. The zinc within the cavity of porphyrin offers the binding site to immobilizing biomimetic $[\text{Fe}_2\text{S}_2]$ catalyst. The integration of a photosensitizer (porphyrin) with a H_2 evolution catalyst (Fe_2S_2 complexes) within one solid materials avoid the using of an electron mediator, where the photo-excited electron from porphyrin can directly transfer to biomimetic $[\text{Fe}_2\text{S}_2]$ catalyst for H_2 production. Due to the efficient photo-excited charges separation and enhanced stability of the di-iron catalyst within the robust MOFs, the H_2 evolution rate and total H_2 production yield of heterogeneous catalytic system was much higher than the similar homogeneous catalytic system.

2,2'-bipyridine-5,5'-dicarboxylic acid is a multi-dentate chelating ligand, can form complexes with many transition metal [74]. It is interesting to synthesize MOFs by using 2,2'-bipyridine-5,5'-dicarboxylic acid as a building blocks, in which the dicarboxylic group is involved in bridging the oxo-metal cluster and the

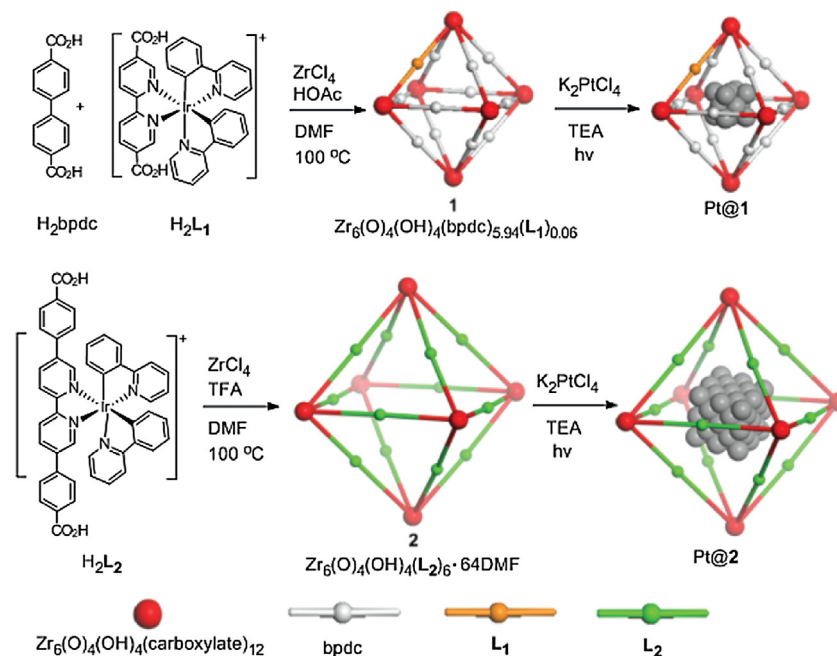


Fig. 8. Schematic for preparation of visible-light responsive MOF-1 using $[\text{Ir}(\text{ppy})_2(\text{bpy})]^+$ -derived dicarboxylate acids H_2L_1 as linkers and MOF-2 by using extended $[\text{Ir}(\text{ppy})_2(\text{bpy})]^+$ -derived dicarboxylate acids H_2L_2 as linkers, and subsequent photocatalytic deposition of Pt nanoparticle within the cavity of MOFs. Reproduced with permission from Ref. [78]. Copyright 2012 American Chemical Society.

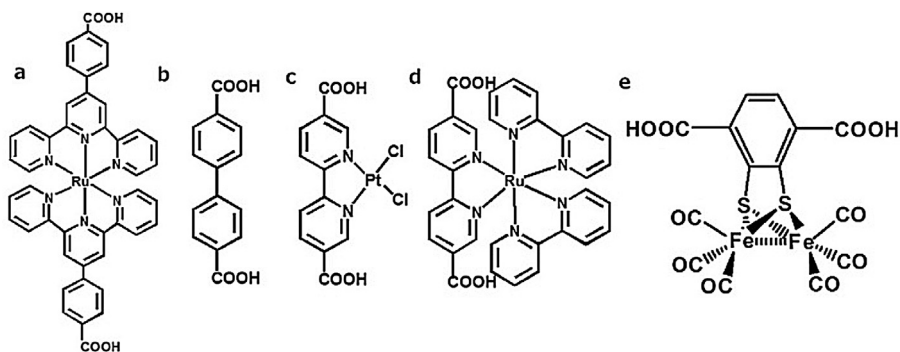


Fig. 9. Building ligands (a) $\text{Ru}(\text{tpy})_2$, (b) bpdc, (c) PtDCBPY, (d) RuDCBPY, (e) $\text{FeFe}(\text{dcbdt})(\text{CO})_6$ as building block of MOFs.

uncoordinated nitrogen donors can be employed to bind the extraneous metal ion [75]. Yaghi and co-workers [76] fabricated MOF-253 through the reaction of oxophilic Al^{3+} ions with 2,2'-bipyridine-5,5'-dicarboxylic acid. The as-prepared MOF-253 has open 2,2'-bipyridine coordination sites which poise for coordinating with transition metal ions. Subsequently, Pd and Cu ions were metalated within the MOF, resulting in the significant enhancement of selectivity for the adsorption of CO_2 over N_2 . Recently, a bifunctional photocatalyst (MOF-253-Pt) for H_2 production from water was designed by Xu et al. [77] through post-modification of immobilizing a platinum complex within such porous 2,2'-bipyridine-based MOFs as shown in Fig. 7. The UV–vis spectra of MOF-253-Pt with the absorption edge of around 650 nm shown red-shift compared with that of MOF-253. An intensive absorption band located around 410 nm was observed, and the color of MOF-253 changed from white to bright yellow after immobilizing a platinum complex, but different from the red color of $\text{Pt}(\text{bpydc})\text{Cl}_2$ complexes. MOF-253-Pt serves both as a photosensitizer for light harvesting and a photocatalyst for H_2 evolution. As shown in Fig. 7b, the photocatalytic activity of H_2 production over MOF-253-Pt significantly enhanced in comparison with the parental MOF-253 under visible light irradiation in the presence of TEOA as sacrifi-

cial electron donor, and 4.7 times of that evolved over complex $\text{Pt}(\text{bpydc})\text{Cl}_2$. The presence of shortly separated Pt–Pt pairs within MOFs-253-Pt, which evidenced by the extended X-ray absorption fine structure (EXAFS) and low temperature luminescence, can be explained for the enhancement of photocatalytic activity. The short electron transfer pathway and enhanced stability of Pt complex anchored within MOF also contributed to promote photocatalytic performance of H_2 production.

However, due to its relatively soft Lewis basic nitrogen donors, a wide variety of transition metals primarily coordinated with the nitrogen donors rather than the hard Lewis basic carboxylates, which limits its application in-situ synthesis of MOFs with uncoordinated nitrogen donors for post-synthetic metalation. Therefore, metalated bipyridine complex was used as building block to in situ construct MOFs with desirable optical properties. Ru, Ir, Re complexes have been directly incorporated into a Zr based MOF without changing their textural structures [67], and Lin and co-workers prepared two visible light responsive MOF-1 and MOF-2 [78]. MOF-1, which built from $[\text{Ir}(\text{ppy})_2(\text{bpy})]^+$ -derived dicarboxylate acids H_2L_1 (2 wt% loading amount) and biphenyldicarboxylated (BPDC) as the bridging ligand and zirconium oxo-cluster as connecting center (Fig. 8), has a large BET surface area ($1194 \text{ m}^2/\text{g}$) and an

average pore size of 6.7 Å. Expanded MOF-2, which constructed from extended ligand H_2L_2 as the bridging ligand and zirconium oxo-cluster as connecting center, has an octahedral cavity with a diameter of 1 nm. Visible light excitation of the resultant MOFs with photoactive $[Ir^{III}(ppy)_2(bpy)]^+$ moiety results in the generation of a 1MLCT excited state, then subsequent followed by a intersystem crossing to form a long-lived 3MLCT state, and finally returns to the ground state through phosphorescent emission. The lifetimes of the 3MLCT for MOF-1 and MOF-2 were determined by time-resolved emission measurements to be 51.8 and 110.3 ns, which were longer than those of corresponding ligands due to the rigidity of the MOF frameworks. By introducing the TEA (triethylamine) as the electron donor to quench the photo-excited $[Ir^{III}(ppy)_2(bpy)]^{+*}$ upon Xe-lamp equipped with 420 nm cutoff filter to produce one electron reduced $[Ir^{III}(ppy)_2(bpy)]^-$ which can be used for reducing PtC_4^{2-} to directly form Pt NPs inside the MOFs pore. The diameter of Pt nanoparticles within the MOF-1 and MOF-2 are found to be 2–3 nm and 5–6 nm, respectively as observed by high-resolution transmission electron microscopy. The photocatalytic performance of the obtained Pt@MOF assemblies was investigated by photocatalytic hydrogen production using TEA as sacrificial under visible light irradiation. The maximum hydrogen evolution turnover number for Pt@1 and Pt@1 was found to be 730 and 1620 under the optimized reaction conditions, respectively. These Pt@MOF assemblies can be reused in 4 times in activity without significantly decreased in activity. The enhanced activity of Pt@MOFs can be primarily attributed to the synergetic effects of two factors, including efficient photo-excited electron transfer from the unstable $[Ir^{III}(ppy)_2(bpy)]^-$ species to Pt nanoparticle, and slowing down the self-decomposition of the Ir complex by the fixation of Ir complexes within MOFs.

Similar to the strategy of synthesizing Ir incorporated MOFs, Matsuoka et al. [79] prepared a Ru-incorporated Ti-based MOF $[Ti-MOF-Ru(tpy)_2]$ by using a bis(4'-(4-carboxyphenyl)-terpyridine)Ru(II) complex (Fig. 9a) as linker. The Ru(II) complex within the MOFs has a wide absorption band in the visible-light region, which allows to *in situ* photocatalytic deposition of Pt nanoparticles as a co-catalyst. Pt nanoparticles deposited Ti-MOF-Ru(tpy)₂ exhibits remarkable photocatalytic activity of H_2 production from water by using TEOA as a sacrificial electron donor under visible-light irradiation even up to 620 nm. Notably, a highly robust MOFs constructed from mixed organic molecular, including 4,4'-biphenyldicarboxylic acid (Fig. 9b), $Pt(dcbpy)Cl_2$ (Fig. 9c), and $[Ru(dcbpy)(bpy)_2]^{2+}$ (Fig. 9d), as linker and Zr ions as connecting centers, was reported by Fu and co-workers [80]. The two metal complexes functionalized MOFs given a high photocatalytic H_2 production in the absence of any electron relay by taking the advantage of facile electron transfer from the Ru complexes (photosensitizer) to the active Pt-complexes (active sites) within one single solid materials. These works demonstrated that the light absorption behavior of MOFs could be rationally tuned by incorporating appropriate light-capturing components, and the active sites for H_2 production also can be varied by immobilizing different active species within MOFs.

Recently, a post-synthetic exchange of MOFs' organic linkers by organometallic compounds has been used to produce the functionalized MOF [81]. A molecular diiron proton reduction catalyst $[FeFe]-(dcbdt)(CO)_6$ (Fig. 9e) has been successfully incorporated into a water-stable Zr-based MOFs by post-synthetic exchange strategy, without disrupting the underlying framework topology. The diiron complexes functionalized MOFs exhibits high efficiency and stability for photochemical H_2 production in the presence of $[Ru(bpy)_3]^{2+}$ as photosensitizer and ascorbate as electron donor. This protocol can be applied to the incorporation of organometal-

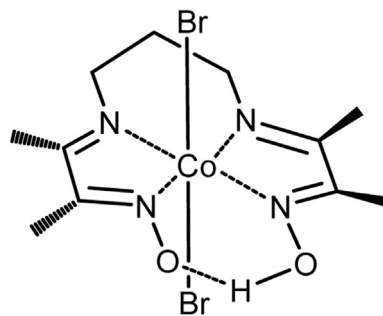


Fig. 10. Molecular structure of a well-defined cobaloxime proton reduction catalyst.

lic compounds with low thermal and chemical stability within the framework of MOFs under mild conditions.

The functionalization of MOFs with organometallic compounds is not only limited on linker modification strategy. The cavity of photo responsive MOFs are also an ideal host matrix for the efficient encapsulation of organometallic species as a proton reduction catalyst through a “Ship-in-a-bottle” strategy. Gascon and co-workers [82] use this method to assembly of a well-defined cobaloxime proton reduction catalyst inside NH_2 -MIL-125(Ti) as a noble-metal-free photocatalyst. The flexible $N^2,N^{2'}$ -propanediylbis(2,3-butanedione 2-imine 3-oxime) ligand was firstly absorbed in the cavity of NH_2 -MIL-125(Ti), followed by introducing $CoBr_2$ under aerobic conditions to yield well-defined cobaloxime proton reduction catalyst (Fig. 10), which incorporated in the cavities of MOFs with a 2.7% loading amount of Co, this loading amount equates to about one cobalt atom per MOF cavity. The as-formed metal complex was restricted within the cavity of MOFs due to the larger molecular size (>6 Å) than the pore (about 6 Å) of MOFs. The photocatalytic performance of Co@MOFs was evaluated in a deoxygenated mixture of acetonitrile (5 mL), TEA (1 mL) and water (0.1 mL) under visible light irradiation. The encapsulated catalyst showed remarkable photocatalytic activity, almost 20-fold higher than the MOF itself, whereas no H_2 was detected in cobaloxime contained homogeneous system in the absence of photosensitizer. A constant TOF of $0.8 h^{-1}$ was maintained over 65 h for Co@MOFs, suggesting a high stability under visible light irradiation conditions. The isotopic study suggested that the produced H_2 was essentially driven from H_2O . The absent EPR signal of Ti^{III} species in Co@MOF demonstrated the efficient charge transfer from the titanium cluster of MOFs to the cobaloxime proton reduction catalyst.

5. Semiconductor/MOFs photocatalysts-driven photocatalytic H_2 production from water

Among various semiconductor photocatalysts for H_2 production from water [83], Cadmium sulfide (CdS), one of the most promising materials, has been intensively investigated due to the suitable positioned conduction band for H_2 production utilizing the abundant visible region of solar energy [84]. However, the fast photo-generated charge recombination rate and the poor chemical stability of pure CdS nanoparticle greatly hinder its photocatalytic performance. The general way to reduce the photo-generated charge recombination rate is loading a co-catalyst on CdS [85], which could accelerate the transfer of photo-generated electron to co-catalyst, or incorporated CdS within porous materials to prevent the aggregation of CdS during the photocatalytic reaction [94]. The high surface area, remarkable crystallinity, and tunable optical properties of MOFs is a promising support for immobilizing CdS. Since the high surface area can well disperse the CdS and avoid the aggregation of CdS nanoparticles, the remarkable crystallinity and

semiconducting properties offer a pathway to facilitate the charge transfer of photo-generated electron from CdS to co-catalyst.

The first example of CdS nanoparticle supported on MIL-101 for water splitting is reported by Sun and co-workers in 2013 [90]. The decoration of CdS nanoparticle on MIL-101(Cr) were carried out through a hydrothermal treatment, in which MIL-101(Cr) was introduced into CdS precursor and followed by hydrothermal treatment. Subsequently, Pt nanoparticles were photo-deposited on CdS/MIL-101(Cr) as co-catalyst. The photocatalytic performance of Pt/CdS/MIL-101(Cr) was evaluated in lactic acid aqueous solution under visible light irradiation. 10 wt.% of CdS loaded Pt/MIL-101(Cr) showed the highest photocatalytic activity among various examined samples such as pure CdS, CdS/MCM-41, CdS/MOF-5 and different amount of CdS loaded MOFs due to the synergistic effect between MIL-101(Cr) and CdS, and almost 20-fold higher efficiencies was obtained than MOF itself. The photo-stability test of CdS/MIL-101(Cr) was examined by consecutive used 4 times without destroying the crystal structure of MOFs, implying considerable stability of CdS/MIL-101(Cr) during the photocatalytic reaction. The advantages of MOFs in enhancing the photocatalytic activity of CdS are that the large specific surface area of MOFs not only effectively suppress aggregation of CdS and well dispersion of the Pt nanoparticles, but also provides more active sites and photocatalytic reaction centers for proton reduction. On the other hand, the semiconducting properties of MOFs allowing the linkers of MOFs partly absorb the incident light, the photo-excited electron from the linker of MOFs firstly transfer to the conduction band of CdS, then to Pt nanoparticle where the reduction of proton takes place on, resulting in enhancing photocatalytic activity.

Due to the lower reduction potential of the excited photosensitizer unit of MIL-101(Cr) than the conduction band of CdS, the photo-excited electron from CdS can only directly transfer from CdS to Pt nanoparticles, which requires more contact area between CdS and Pt nanoparticle. To further promote the transfer of photo-generated electrons from CdS to Pt nanoparticles, UiO-66, which has higher reduction potential of the excited photosensitizer unit than that of CdS, has been employed as support to *in situ* grown CdS nanoparticles upon the light irradiation, reported by Yuan and co-workers [88]. The photocatalytic activity for H₂ production over 16 wt% CdS supported UiO-66 can reach to 47 mmol h⁻¹ g⁻¹ in the presence of L-ascorbic acid as sacrificial agent and Pt nanoparticle as co-catalyst, corresponding to 1.2% quantum efficiency under 420 nm irradiation, which is much higher as compared to g-C₃N₄/CdS, TiO₂/CdS, bare CdS, and UiO-66. The enhanced photocatalytic H₂ evolution is explained by the increased interfacial charge transfer pathway from CdS to UiO-66 then to Pt nanoparticles. The shorter PL lifetime in CdS supported UiO-66 than that of pure CdS and the enhanced 2-fluorescence intensity of hydroxyl-terephthalic acid produced by the reaction of terephthalic acid with hydroxyl radicals over CdS supported UiO-66 under light irradiation in basic solution confirm the fast transfer of photo-generated electrons from CdS to UiO-66, leading to the efficient charge separation of electron-hole pairs, finally promoting the photocatalytic H₂ production.

As well known that Pt nanoparticles play an important role in photocatalytic H₂ production [95]. However Pt is scarce with very high cost. In order to reduce the amount of Pt metals used in photocatalytic H₂ production system, MoS₂ as a promising alternative to Pt for H₂ evolution from water, has been photo-deposited on CdS/UiO-66 by Wu and co-workers (noted as MoS₂/U6-CdS) [89], with the aim to promote the interfacial electron transfer efficiency and enhancing the photocatalytic H₂ production. The photocatalytic H₂ production activity of MoS₂/U6-CdS was investigated in an aqueous solution containing lactic acid as sacrificial agent under visible light irradiation. 50 wt% CdS loaded UiO-66 exhibits 515.4 mmol h⁻¹ H₂ production rate in the presence of 1 wt% MoS₂,

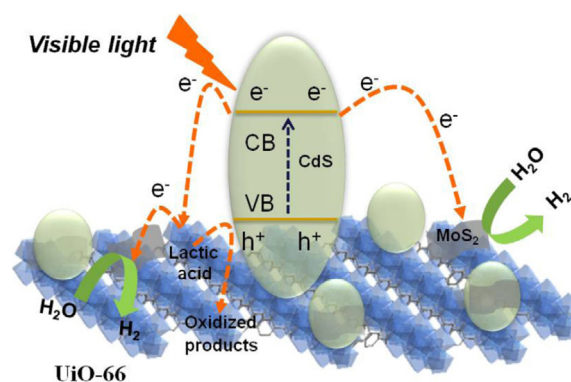


Fig. 11. Schematic illustration of a possible mechanism for photocatalytic H₂ production from water over MoS₂/U6-CdS. Reproduced with permission from Ref. [89]. Copyright 2015 Elsevier.

which is almost two times higher than that produced over 1 wt% Pt loaded U6-CdS at same reaction conditions. The optimum loading amount of CdS and MoS₂ are ≈ 50 wt% and ≈ 1.5 wt%, reaching to 650 mmol h⁻¹, this is corresponding to 23.6% quantum efficiency under 420 \pm 10 nm irradiation. The synergic action of CdS, UiO-66, and MoS₂ has been proposed and illustrated in Fig. 11. The electrons generated upon the absorption of visible light by CdS can not only inject into the LUMO state of UiO-66, then transfer to the MoS₂, but also directly inject into the conduction bands of MoS₂, finally the proton reacts with electron to produce H₂ on MoS₂. Meanwhile, the lactic acid donates electrons to the valence band of CdS to consume the holes. The enhancement of the photocatalytic activity and stability of MoS₂/U6-CdS can be attributed to cooperative promoting effect from both U6-CdS and MoS₂ in the formation of well dispersed MoS₂ and CdS, promoting the separation of photogenerated charge carriers efficiently by forming the heterojunction between CdS and MOFs, and increasing the electron transfer pathway as well as active sites by photocatalytic deposition of MoS₂. These works proposed a new way for the fabrication of other high efficient MOFs/semiconductor photocatalysts for H₂ production, as summarized in Table 1. However, the semiconductor loaded on MOFs for water splitting are mainly focused on CdS, other cost-affordable, highly active semiconductor with suitable redox abilities supported on MOFs should be discovered to improve the photocatalytic activities of various redox reactions.

6. Dye-sensitized MOFs-involved H₂ production system

Photo-sensitization can also be realized by using an organic dye as sensitizer to absorb light energy, convert it into chemical energy, and then transfer the chemical energy to nearby catalytic active site to drive redox reaction. Over past 30 years, organic dye sensitized catalyst has been demonstrated as an important approach for the development of visible light-responsive photocatalysts for H₂ production in consideration of their tunable HOMO state and LUMO state by anchoring different ligands [96,97]. Considering the present photosensitizers-involved photocatalytic H₂ production system, they can be classified into metal-free organic dyes and coordination metal-organic complexes. Since many reported metal complex dyes are mainly focused on expensive Ru-, Pt-, Re-, and Ir- based complexes, metal-free organic dyes display low-cost, variety, and tunable structures, have attracted little attention [66]. According to the reported studies in the literature, plentiful metal free organic dyes such as eosin Y (EY) [98], rose bengal (RB) [99], rhodamine B (RhB) [100], erythrosine B (ErB) [101] are used in dye-sensitized H₂ production system. Despite the numerous advantages displayed by metal-free organic dyes, there are still suffered from many problems such as low stability (dissolution

Table 1
Summaries of MOF-semiconductor-based photocatalysts for H₂ production from water. [a] Reduced graphene oxide; [b] without co-catalyst.

MOFs	Semiconductor	Co-catalyst	Sacrificial agent	H ₂ production rate (mmol h ⁻¹ g ⁻¹)	Ref.
MIL-101(Cr)	CdS	Au	Na ₂ S/Na ₂ SO ₃	25	[86]
UiO-66	CdS	Pt, RGO ^a	Na ₂ S/Na ₂ SO ₃	2.09	[87]
UiO-66	CdS	Pt	L-ascorbic acid	47	[88]
UiO-66	CdS	MoS ₂	Lactic acid	32.5	[89]
MIL-101(Cr)	CdS	Pt	Lactic acid	≈7.5	[90]
Cd-MOF	CdS, TiO ₂	None ^b	Na ₂ S/Na ₂ SO ₃	≈1.6	[91]
UiO-66	g-C ₃ N ₄	None ^b	L-ascorbic acid	≈1.4	[92]
ZAVCl-MOF	CdS	Pt	Ethanol	≈0.5	[93]

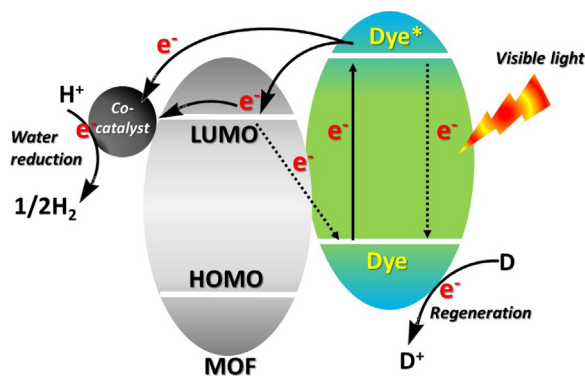


Fig. 12. Proposed mechanism of a dye-sensitized MOFs involved photocatalysis for H₂ production from the water under visible light irradiation.

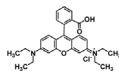
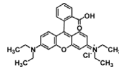
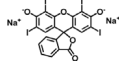
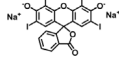
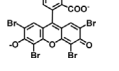
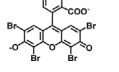
and self-degradation), fast carrier recombination and deactivation. One typical way to improve the efficiency of photosensitization is immobilizing the dye onto the porous semiconductor materials to avoid self-degradation and suppress carrier recombination rate by injecting the photo-excited charges to conduction band of semiconductor, and from semiconductor to co-catalyst for proton reduction [102,103]. MOFs are typical crystalline porous material, which built from organic ligands and metal clusters. Most of organic ligands used to cross-link metal clusters have benzene ring. Up to now, Most of reported MOF-based photocatalytic H₂ production systems suffer from poor visible light utilization, high cost, low activity and instability. Fortunately, the large surface area as well as unique organic properties is beneficial for physical and chemical absorption of organic dye via strong π - π stacking between the benzene rings of both MOFs and dyes, and Van Der Waals interaction, which is highly important for promoting the electron transfer from dye to co-catalyst. Additionally, the metal clusters of the MOFs can also serve as active site to accept the photo-excited electron from dye and carry out the photon reduction reaction. MOFs become potential candidate of an advanced co-catalyst for improving the photocatalytic performance of the dye-sensitized H₂ production system.

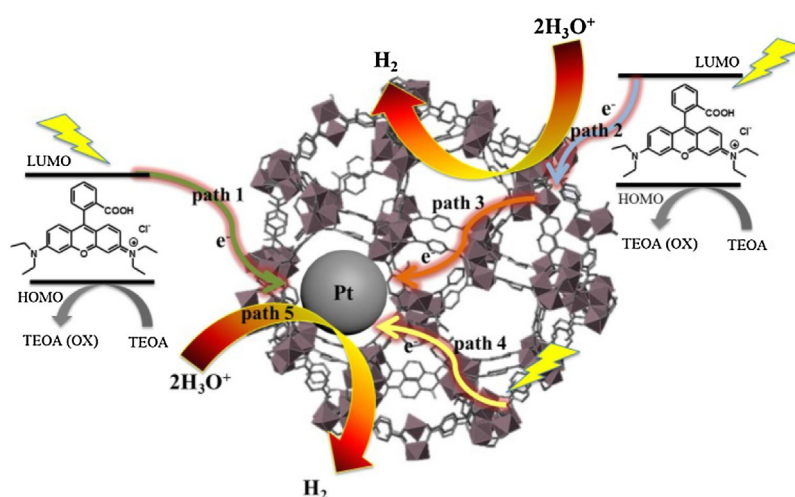
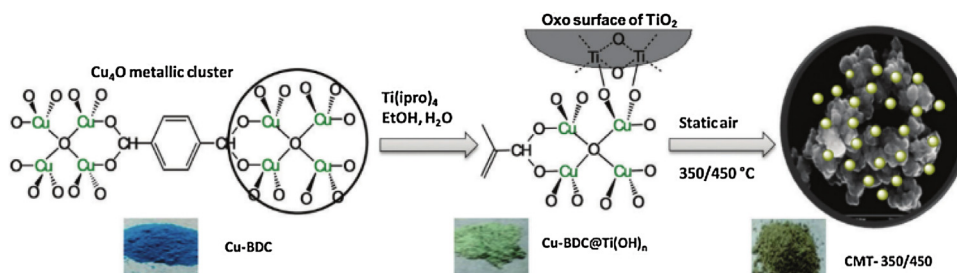
As shown in Fig. 12, dye sensitized MOFs-involved photocatalytic H₂ production system composed of metal free organic dye as photosensitizer, a sacrificial reagent as an electron donor, and a metal nanoparticle supported MOFs as co-catalyst. The incident light with energy higher than the band gap of dye excite one electron from HOMO state to LUMO state of dye. The photo-excited electrons transfer occurs not only to the metal nanoparticle but also inject into the LUMO state of MOFs, subsequently followed by migration of the LUMO state's electrons to the surface's metal nanoparticles, finally the participating in the reduction of water. The oxidized dyes molecules then come back to its original state by receiving electrons from the sacrificial reagent. However, the back electron transfer, fluorescence decay of excited dye molecule and possible recombination pathways from LUMO state's electrons to HOMO state of dye molecule, accompanied with the photon

reduction process [104]. Therefore, reducing the metal nanoparticle size and increasing the contacting interface between the dye and the co-catalyst is an efficient way to prevent the back electron transfer. In this section, the summarization of metal free organic dye-sensitized MOFs involved H₂ production system were conducted in detail (Table 2).

Yamashita and co-workers report Rhodamine B dye to sensitize amine-functionalized chromium based MIL-101(Cr) with imbedded Pt nanoparticles for photocatalytic H₂ production [105], and the photocatalytic activities of the catalysts were evaluated in the presence of TEOA as sacrificial agent. The pristine MOF is inactive for H₂ evolution, where slight reaction occurred after introducing RhB into reaction solution, which demonstrated that the metal cluster can serve as an active site to accept photo-generated electron from dye and drive the proton reduction reaction. Significant enhancement on H₂ evolution rate was observed when Pt nanoparticle was imbedded into MOFs due to the efficient charge transfer from dye to Pt/MOFs. The decrease in the fluorescence intensity of RhB solution containing TEOA and Pt/MOFs confirms the fast transfer of photo-generated electrons from dye to Pt/MOFs. The highest H₂ evolution rate was obtained as 0.57 mmol h⁻¹ g⁻¹ while the Pt loading amount was 1.5 wt%, which is higher than 1.5 wt% Pt loaded anatase TiO₂ and mesoporous SiO₂ in the identical conditions. The synergistic effect between Pt nanoparticles and MOFs is the main reason for attaining high photocatalytic activity compared with other supports. The possible photo-excited electron transfer pathway is illustrated in Fig. 13. Under visible light irradiation, RhB absorbs light photon to generate electron from its HOMO state to LUMO state. The excited electrons will most likely transfer to the LUMO state of MOFs. When the Pt nanoparticle was loaded on MOFs, a Schottky barrier can form at the interface of MOFs and Pt nanoparticle due to the higher work function of Pt than MOFs, which cause the electron gathered in the LUMO state of MOFs transfer to the Pt nanoparticles. On the other hand, the direct excited electron transfer from dye to Pt nanoparticle also can be realized when RhB is colliding with Pt nanoparticles, finally proton received electron on the surface of Pt nanoparticles to produce H₂. In addition, MOFs can also serve as semiconductor to partially absorb visible light to generate electrons for H₂ evolution. Meanwhile, the regeneration of oxidized RhB is achieving by getting electrons from TEOA. The roles of MOFs in facilitating the electron transfer, protecting the photosensitizer, reducing the self-quenching of RhB and stabilizing the Pt nanoparticles is essentially important for attaining high photocatalytic activity. Similar to the strategy of using RhB as photosensitizer to induce H₂ production from water, Yan's group [106] also used RhB to sensitize water stable UiO-66 by adsorbed or directly added RhB into H₂ production system. Remarkable H₂ evolution rate also observed while using Pt nanoparticle as co-catalyst and TEOA as electron donor under visible light irradiation. Very recently, Xue and co-worker used Erythrosin (ErB) to sensitize water stable UiO-66 for H₂ production, and the highest H₂ evolution rate is obtained as 0.46 mmol h⁻¹ g⁻¹ in the condition of using 30 mg ErB as photosensitizer and Pt as co-catalyst under visible light irradiation [108].

Table 2
Summaries of dye-sensitized MOFs-involved H₂ production system.

MOFs	Dye	Co-catalyst	Sacrificial agent	H ₂ production rate (mmol h ⁻¹ g ⁻¹)	Ref.
MIL-101(Cr)		Pt	TEOA	0.57	[105]
UiO-66		Pt	TEOA	0.116	[106]
MIL-101(Cr)		Ni@NiOx	TEOA	6.25	[107]
UiO-66		Pt	L-ascorbic acid	0.46	[108]
MOF-5		Ni	TEOA	30.22	[109]
MIL-101		Ni-Mo	TEOA	14.8	[110]

**Fig. 13.** illustrated the possible photo-excited electron transfer pathway. Reproduced with permission from Ref. [105]. Copyright 2014 Royal Society of Chemistry.**Fig. 14.** Schematic illustration of MOF-templated synthesis of Cu/CuO@TiO₂ nanocomposite. Reproduced with permission from Ref. [114]. Copyright 2014 Royal Society of Chemistry.

It seems that the reaction of proton reduction mainly take place on the surface of metal nanoparticles, and it is reasonable to image that significant enhancement can be observed while the combination between dye and metal nanoparticles increased. This can be achieved by introducing a large number of tiny metal nanoparticles within H₂ production system. According to the previous researches, Pt nanoparticles have presented superior physical and chemical properties for H₂ production due to its low over-potential. However, they are still expensive. Lu and co-workers founded that

small-sized Ni with exposed (111) facet can acted as an advanced co-catalyst for constructing an efficient photocatalytic H₂ production system [109]. MOF-5 has been selected as support to well dispersed Ni nanoparticles (Ni@MOF-5) due to its high specific surface area (2973 m² g⁻¹). The over-potential of Ni@MOF-5 was measured to be −0.37 V by electrochemical measurement, which is close to that of Pt@MOF-5. The photocatalytic reaction was investigated by using Eosin Y (EY) as photosensitizer and TEOA as electron donor, and the hydrogen evolution rate of Ni@MOF-5 was obtained

as $30.22 \text{ mmol h}^{-1} \text{ g}^{-1}$ at optimized reaction condition, which was comparable to Pt@MOF-5, but much higher than SiO_2 , Al_2O_3 supports at same metal loading amount under the identical condition. The large capacity of MOFs for absorbing EY, strong interaction between MOFs and dye, the semiconducting properties of MOFs, the high loading amount of Ni nanoparticles, and the low overpotential of Ni@MOF-5 are all accounted for the high photocatalytic performance for H_2 evolution. Additionally, similar H_2 production system were demonstrated by Xue and co-workers with their ErB sensitized Ni@NiO_x@MOFs by in situ photo-deposition of Ni@NiO_x on MIL-101 framework [107]. More recently, NiMo alloy nanoparticle loaded on MIL-101 (NiMo@MIL-101) were also prepared for photocatalytic H_2 production from water [110], and the results found that NiMo@MIL-101 exhibited extremely higher photocatalytic activity than mono metal nanoparticle loaded MIL-101, due to the lower H_2 adsorption free energy than that of Ni and Mo. These works suggested that the dye sensitized MOFs displayed great potential for photocatalytic H_2 production and brought new chance to develop highly efficient dye sensitized MOFs-involved photocatalytic system for H_2 production.

7. MOF templated nanocomposite for photocatalytic H_2 production from water

Heterojunction, the junction between two different semiconductor materials, is an attractive bandgap engineering technique to suppress the recombination rate of photogenerated holes and electrons, leading to a multi-fold increase of the photocatalytic activity [111]. Numerous attentions has been paid to the design and development of heterojunction photocatalysts for H_2 production from water [83]. One of the promising strategies is using MOF as template to synthesize heterojunction photocatalysts. MOF is one member of crystalline inorganic-organic polymers with high porosity. Most of the connecting centers in MOFs structure are transition metals with empty outside orbitals. These connecting centers are considered as Lewis acid, which can form coordination bonds with organic linker by receiving electrons from organic linker. The spatial structure of MOFs is varied from the type of transition metals and linkers. It is easy to understand that the heterojunction photocatalysts can be obtained by the calcination or carbonization of two transition metals ions contained MOF. For example, Fe_2O_3 @ TiO_2 nanocomposite was synthesized through calcination of core-shell MIL-101@ TiO_2 under air condition at 550°C [112]. The transformation of MIL-101 to Fe_2O_3 is evidenced by the color changing and PXRD pattern of samples. High resolution TEM suggested that the morphology of nanocomposite is well maintained after the calcination. The as-formed nanocomposites is applied to drive H_2 production from water by using trimethylamine as a sacrificial agent and Pt nanoparticles as co-catalyst under visible light irradiation. The Fe_2O_3 @ TiO_2 nanocomposite displayed remarkable photocatalytic activity and can be recycled for three times without the decrease of catalytic activity and destroying the crystal structure, indicating the high stability of Fe_2O_3 @ TiO_2 nanocomposite. Subsequently, Do et al. [113] used similar strategy to prepare hollow Fe_2O_3 - TiO_2 - PtO_x photocatalyst for H_2 production from water by using Fe-based MOFs as sacrificial template.

Very recently, Pal's group [114] synthesized a novel Cu/CuO@ TiO_2 heterojunction nanocomposites (CMT-350/450) by using a Cu-based MOF as sacrificial template as illustrated in Fig. 14. The Ti isopropoxide ($\text{Ti}(\text{ipro})_4$) was used as Ti precursor prior absorbed on MOF in an ethanol and water mixture, and keep stirring for 12 h to allow the completely hydrolysis of Ti, then followed by carbonization to obtain powder Cu/CuO@ TiO_2 under static air atmosphere. The photocatalytic evaluation of Cu/CuO@ TiO_2 nanocomposites were performed for photocatalytic

H_2 production from water in the presence of electron donor under solar light irradiation. It was found that the nanocomposites with 0.5 wt% Cu loading amount showed the best photocatalytic activity, and the maximum H_2 generation rate is $286 \text{ mmol g}^{-1} \text{ h}^{-1}$, which is higher than that of CuO loaded TiO_2 prepared by an impregnation method. The small size of Cu nanoparticle and heterojunction formed between CuO and TiO_2 are two important factors in attaining high photocatalytic activity by suppressing the recombination rate of photogenerated holes and electrons. This novel method also applied to prepare Co_3O_4 / TiO_2 heterojunction nanocomposites [115] for photocatalytic H_2 production from water by using a Co-based MOF as sacrificial template. Furthermore, several porous carbon/metal oxide nanocomposites were prepared by the carbonization of MOFs under inert atmosphere condition and served as efficient and low-cost electrocatalysts for water splitting [116–118]. These achievements imply that the synthesis of MOF templated heterojunction nanocomposites is a novel method for the design of many advanced photocatalysts capable of providing high efficiency for solar-energy conversion.

8. Metal nanoparticle loaded MOFs for visible light enhanced H_2 production from hydrogen storage materials

The efficient storage and transportation of H_2 is a great challenge. A safe and efficient method is to store hydrogen in the form of liquid or solid materials under ambient conditions, and the stored hydrogen can be release at certain condition. Therefore, much attention has been paid to the design of efficient catalysts for in-situ H_2 releasing from hydrogen storage materials. MOF has emerged as an interesting platform to load metal nanoparticle due to unique physical and chemical properties [119–121]. The optical and electrical properties arising from the delocalized nature of organic ligand orbitals, and the porosity of MOF enable them to fine tune the size and electron density of metal nanoparticles, as the catalytic performance strongly depends on the size and electron density of metal nanoparticle [122–124]. The charges generated upon light irradiating on MOF as well as the active species generated during the reaction process can photocatalytically promote intrinsic activity of metal nanoparticle [125].

The first example for visible-light-enhanced H_2 production from ammonia borane (NH_3BH_3) using Pd nanoparticle supported MOF was contributed by Yamashita et al. in 2014 [126]. The Ce doped Cr based MOF (CeMIL-101) with size around 50 nm were prepared by hydrothermal treatment. The aim of doping Ce in Cr based MOF is to accelerate the transportation of photogenerated electron from MOF to Pd nanoparticle by recycling $\text{Ce}^{4+}/\text{Ce}^{3+}$ redox. X-ray diffraction and X-ray adsorption measurements confirmed the presence of $\text{Ce}^{4+}/\text{Ce}^{3+}$ redox within MOF, with a large amount of Ce^{4+} . TEM images reveal that very tiny Pd nanoparticles with diameter around 2.7 nm are well dispersed on MOFs with (Pd/CeMIL-101) and without Ce doping (Pd/MIL-101). The catalytic activities of Pd/MIL-101 and Pd/CeMIL-101 yielded same H_2 amount due to the similar Pd nanoparticle size. It was noted that visible light irradiated catalytic reaction could greatly enhance the catalytic activity as compared to the dark conditions. $108 \mu\text{mol}$ and $378 \mu\text{mol}$ enhancement was observed for sample Pd/MIL-101 and Pd/CeMIL-101 under visible light irradiation, respectively. Apparently, the H_2 evolved over Pd/CeMIL-101 is two times of the H_2 evolved over Pd/MIL-101, evidencing that the doped Ce is essentially important for photocatalytically promoting the intrinsic catalytic activity of Pd nanoparticle (Fig. 15). The catalytic activity dramatically decreased while introducing hydroxyl radical scavenger (2-propanol) into reaction solution. The promoting effect of doped Ce on the formation of hydroxyl radical demonstrated by fluorescence study. However, increasing the concentration of super-

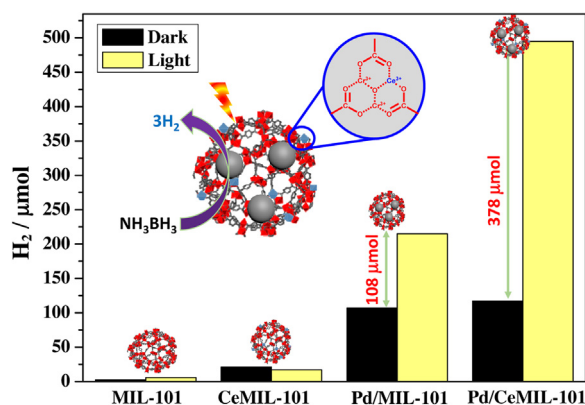


Fig. 15. Hydrogen production from ammonia borane dehydrogenation on different catalysts under dark conditions and visible light irradiation (600 μmol H₂ represents approximately 100% conversion of ammonia borane).

oxide anion by bubbling O₂ into the reaction solution, the H₂ production rate increased. These results suggested that the photo-generated charges have positive effect on breaking down the B–N bond of ammonia borane. Moreover, the process of photogenerated electron migration from MOF to Pd nanoparticle can be accelerated by recycling Ce⁴⁺/Ce³⁺ redox. This work offers the guideline and strategy to develop high efficient and economic catalyst for H₂ production from ammonia borane.

Very recently, plasmonic Au@Pd nanoparticles on Ti ions doped Zr-based MOFs catalyst has been design for synergistic boosting of H₂ production from formic acid under visible light irradiation [127]. This novel hybrid catalyst displayed a high H₂ production rate of 42000 mL h^{−1} g^{−1} (Pd), corresponding to the turnover frequency (TOF) of 200 h^{−1} based on Pd. The high catalytic activity can be attributed to that the dissociation of C–H bonds and O–H bonds of Formic acid are promoted by a large number of –NH₂ groups anchored within MOFs as well as electron rich Pd nanoparticles induced by photoactive MOFs and plasmonic effect of Au under visible light irradiation.

Apart from the noble based catalysts, non-noble-metal supported MIL-101 (Co/MIL-101, Ni/MIL-101, Cu/MIL-101) were also prepared for photocatalytically enhancing the ammonia borane dehydrogenation [128]. The catalytic activities of those noble-metal free catalysts under visible light irradiation are considerably higher than that under dark conditions as shown in Fig. 16. The corresponding turnover frequency is comparable to or even higher than that of noble metal nanoparticles driven ammonia borane dehydrogenation. The recycling experiment demonstrated the high stability of these samples. This work offers a new strategy for developing low-cost and highly effective catalyst for ammonia borane dehydrogenation. MOF has been proved to be useful for photocatalytically promoting the reaction of H₂ generation from hydrogen storage materials due to its unique properties).

8. Summary and outlook

In this review paper, the most recent innovative strategies to the development of MOF-based photocatalysts with high efficiency and durability toward H₂ production from water and hydrogen storage materials were summarized in detail. Based on the different photocatalytic H₂ production systems, MOFs played as the pure photocatalysts, or as support for loading metal nanoparticle, photosensitizer or semiconductor for H₂ production from water and hydrogen storage materials. Very distinct results have been reported in the past few years. These achievements have demonstrated that MOFs are a new class of promising porous materials integrating the functional organic linker with active site

in an organized manner to realize efficient light harvesting and photocatalytic H₂ production. Compared with conventional photocatalysts, MOF has the following advantages: (i) controllability, the cavity and pore size of MOF can be changed by rational design, enable MOF offering significant chemical diversity. Furthermore, the molecular nature of MOF provides an idea platform for well organizing multiple components in a single solid. (ii) high surface area and porosity, these properties facilitates the diffusion of sacrificial agent and proton through the open channels as the mobility of proton and sacrificial within catalyst is highly important for achieving excellent photocatalytic performance. Tiny semiconductor, metal nanoparticle as well as metal-free dye molecular can be well dispersed into MOF. (iii) extremely short charge transportation pathways, the atomic-level crystal structure of MOF significantly reduce the distance of charge transportation pathway to active sites. The involvement of MOF-based materials into photocatalysis has opened up new avenues for the efficient conversion of the solar energy into chemical energy for driving redox reactions. However, the study of MOF-based photocatalysts in this field is still in its early stage. There are several problems still needed to be solved in the coming years.

First, in the case of H₂ production from water, electron donor is an indispensable reagent. The dye regeneration by receiving an electron from electron donor are closely related to the sustainable H₂ production. When the photosensitizer is used as organic linker to build the MOF, an extremely high concentration of photosensitizer is located within the pore and cavity space, but the problems of electron donor diffusion and proton migration should be considered during the photocatalytic H₂ production process. Depending on the size of electron donor, photosensitizer, and electron mediator, the pore size of utilized MOF should be large enough to allow adequate diffusion of those molecules to the immobilized active sites. In addition, the pore and cavity of MOF are very easily occupied by organic solvent or organic linker and the electron donor is usually in large molecules size. This will prevent the quenching of excited photosensitizer and proton reduction reaction. The method for activation and purification of MOF should be explored to remove the un-reacted organic linker and solvent.

Second, although MOF is a porous crystalline material, light penetration and scattering limited its future application, synthesis of order porous MOF or nanosized MOF is turned to be a solution. Furthermore, most of the studied MOF-based photocatalytic H₂ production systems need sacrificial agent. The catalytic activity significantly decreased once the sacrificial agent is removed. In addition, sacrificial agents are usually hydrogen carrier materials, which makes the reaction system inefficiency and high cost. The sustainable and renewable way is to design an overall photocatalyst by integration of water oxidation active site with water reduction active site within MOF, which can avoid the use of sacrificial agent. Therefore, a lot of problems, such as the selection of electron mediate, band alignment, the architecture of MOF and the interfacial structure should be clarified for efficient charge separation.

Third, dye-sensitized/MOFs and Semiconductor/MOFs photocatalysts-driven photocatalytic H₂ production system have many attractive properties and considerable achievements were obtained. However, those H₂ production systems can't be commercialized because of difficulties associated with instability, harmful to environment, and separating problems. It is of great challenge to search environmental benign alternatives to those photosensitizers with excellent photocatalytic performance and high stability. Since many MOF involved H₂ production systems heavily rely on the noble metal as cocatalyst. Thus, the development of new photocatalysts by using non-noble metal nanoparticles as cocatalysts is of critical importance to achieve economic H₂ production system.

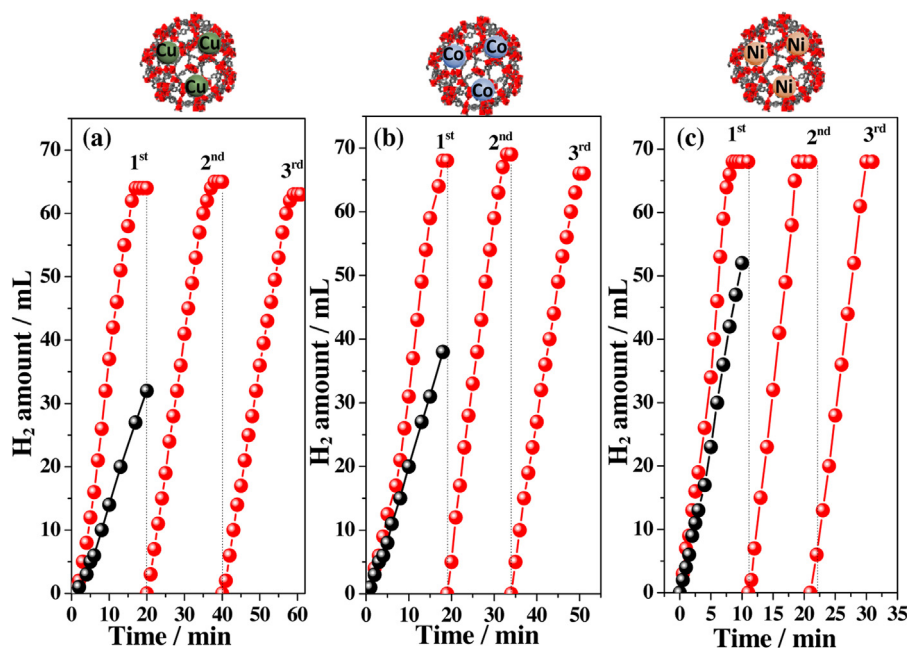


Fig. 16. (a) Hydrogen production from ammonia borane dehydrogenation on different catalysts under dark conditions (black) and visible light irradiation (red) over (a) Cu/MIL-101, (b) Co/MIL-101, and (c) Ni/MIL-101. (For interpretation of the references to colour in this figure legend, the reader is referred to the web version of this article.)

Last but not the least, the poor stability of MOF during the photocatalytic reaction is another critical problem which further hinder its application. In the view of green chemistry, the photocatalytic H_2 production reaction seems necessarily carried out in aqueous solution. The photogenerated active species, such as superoxide anions and hydroxyl radicals are harmful for MOF structure. Recent examples of MOFs are based on transition metal ions such as, Zr^{4+} , Ti^{4+} , Al^{3+} , Cr^{3+} and Zn^{2+} with carboxylate or imidazolate linkers. Although they display modest stability in aqueous solution, the H_2 production efficiency is still low. In general, the stability of MOF is highly depends on the coordination number and local chemical environment, thus optimizing the coordination between metal ions and organic linker is of great importance. The preparation method also affects the stability of MOF, thus looking for the suitable preparation method is quite important. In particular, most of reported MOFs show poor electronic conductivity, which hampers the photogenerated electron transfer. Similar to the photocatalysts in general, doping with non-metal or metal ions within MOF is a feasible method. New directions in the development of photoactive MOFs with high stability to achieve high photocatalytic activity should be proposed and anticipated.

Although the application of photoactive MOF for photocatalytic H_2 production still in their infancy, the significant progress of photocatalytic application of MOF in the past years was already witnessed. Owing to the unique property of MOF, we are confident that MOF can be served as powerful material applied for constructing the sustainable society in near future especially in photocatalytic H_2 production.

Acknowledgements

The present work was partially supported by Grants-in-Aid for Scientific Research (Nos. 26220911, 25289289, 26630409 and 26620194) from the Japan Society for the Promotion of Science (JSPS) and MEXT. YK, KM and HY thank MEXT program “Elements Strategy Initiative to Form Core Research Center”. TA also thanks his financial supporting from NSFC (41425015).

References

- [1] Z.B. Yang, J. Ren, Z.T. Zhang, X.L. Chen, G.Z. Guan, L.B. Qin, Y. Zhang, H.S. Peng, *Chem. Rev.* 115 (2015) 5159–5223.
- [2] M.R. Hoffmann, S.T. Martin, W.Y. Choi, D.W. Bahnemann, *Chem. Rev.* 95 (1995) 69–96.
- [3] T. Hisatomi, J. Kubota, K. Domen, *Chem. Soc. Rev.* 43 (2014) 7520–7535.
- [4] H.F. Cheng, M.C. Wen, X. Ma, Y. Kuwahara, K. Mori, Y. Dai, B. Huang, H. Yamashita, *J. Am. Chem. Soc.* 138 (2016) 9316–9324.
- [5] D.S. Bhatkhande, V.G. Pangarkar, A. Beenackers, *J. Chem. Chem. Technol. Biotechnol.* 77 (2002) 102–116.
- [6] K. Fukui, R. Hayashi, S. Takakura, T. Kamegawa, K. Mori, H. Yamashita, *Angew. Chem. Int. Ed.* 52 (2013) 7446–7450.
- [7] H.F. Cheng, X.F. Qian, Y. Kuwahara, K. Mori, H. Yamashita, *Adv. Mater.* 27 (2015) 4616–4621.
- [8] T. Kamegawa, Y. Shimizu, H. Yamashita, *Adv. Mater.* 24 (2012) 3697–3700.
- [9] A. Fujishima, K. Honda, *Nature* 238 (1972) 37–38.
- [10] M.N. Chong, B. Jin, C.W.K. Chow, C. Saint, *Water Res.* 44 (2010) 2997–3027.
- [11] T. Kamegawa, D. Yamahana, H. Seto, H. Yamashita, *J. Mater. Chem. A* 1 (2013) 891–897.
- [12] H. Kisch, *Angew. Chem. Int. Ed.* 52 (2013) 812–847.
- [13] S. Gunes, H. Neugebauer, N.S. Sariciftci, *Chem. Rev.* 107 (2007) 1324–1338.
- [14] S.Y. Dong, J.L. Feng, M.H. Fan, Y.Q. Pi, L.M. Hu, X. Han, M.L. Liu, J.Y. Sun, J.H. Sun, *RSC Adv.* 5 (2015) 14610–14630.
- [15] W.Q. Li, X. Liu, H.X. Li, *J. Mater. Chem. A* 3 (2015) 15214–15224.
- [16] Y.N. Huo, Z.F. Bian, X.Y. Zhang, Y. Jin, J. Zhu, H.X. Li, *J. Phys. Chem. B* 112 (2008) 6546–6550.
- [17] Z. El Koura, M. Cazzanelli, N. Bazzanella, N. Patel, R. Fernandes, G.E. Arnaoutakis, A. Gakamsky, A. Dick, A. Quaranta, A. Miotello, *J. Phys. Chem. B* 120 (2016) 12042–12050.
- [18] H. Choi, D. Shin, B.C. Yeo, T. Song, S.S. Han, N. Park, S. Kim, *ACS Catal.* 6 (2016) 2745–2753.
- [19] M.C. Wen, P.J. Liu, S. Xiao, K. Mori, Y. Kuwahara, H. Yamashita, H.X. Li, D.Q. Zhang, *RSC Adv.* 5 (2015) 11029–11035.
- [20] S.W. Cao, F. Tao, Y. Tang, Y.T. Li, J.G. Yu, *Chem. Soc. Rev.* 45 (2016) 4747–4765.
- [21] F.E. Osterloh, *Chem. Soc. Rev.* 42 (2013) 2294–2320.
- [22] D.Q. Zhang, M.C. Wen, S.S. Zhang, P.J. Liu, W. Zhu, G.S. Li, H.X. Li, *Appl. Catal. B* 147 (2014) 610–616.
- [23] S.T. Nishanthi, S. Iyyapushpam, B. Sundarakannan, E. Subramanian, D.P. Padiyan, *J. Power Sources* 274 (2015) 885–893.
- [24] X.J. Lang, X.D. Chen, J.C. Zhao, *Chem. Soc. Rev.* 43 (2014) 473–486.
- [25] G.S. Li, Z.C. Lian, W.C. Wang, D.Q. Zhang, H.X. Li, *Nano Energy* 19 (2016) 446–454.
- [26] D.Q. Zhang, G.S. Li, H.X. Li, Y.F. Lu, *Chem. – Asian J.* 8 (2013) 26–40.
- [27] H.F. Cheng, T. Kamegawa, K. Mori, H. Yamashita, *Angew. Chem. Int. Ed.* 53 (2014) 2910–2914.
- [28] K. Mori, M. Kawashima, M. Che, H. Yamashita, *Angew. Chem. Int. Ed.* 49 (2010) 8598–8601.
- [29] A. Kubacka, M. Fernandez-Garcia, G. Colon, *Chem. Rev.* 112 (2012) 1555–1614.

- [30] H.Y. Kohsuke Mori, Chem. – Eur. J. 22 (2016) 11122–11137.
- [31] M. Martis, K. Mori, K. Fujiwara, W.S. Ahn, H. Yamashita, J. Phys. Chem. B 117 (2013) 22805–22810.
- [32] Q.L. Zhu, Q. Xu, Chem. Soc. Rev. 43 (2014) 5468–5512.
- [33] T. Zhang, W.B. Lin, Chem. Soc. Rev. 43 (2014) 5982–5993.
- [34] S.B. Wang, X.C. Wang, Small 11 (2015) 3097–3112.
- [35] J.L. Wang, C. Wang, W.B. Lin, ACS Catal. 2 (2012) 2630–2640.
- [36] K.K. Tanabe, S.M. Cohen, Chem. Soc. Rev. 40 (2011) 498–519.
- [37] M.S. Denny, S.M. Cohen, Angew. Chem. Int. Ed. 54 (2015) 9029–9032.
- [38] M. Kim, J.F. Cahill, H.H. Fei, K.A. Prather, S.M. Cohen, J. Am. Chem. Soc. 134 (2012) 18082–18088.
- [39] P. Deria, J.E. Mondloch, O. Karagiari, W. Bury, J.T. Hupp, O.K. Farha, Chem. Soc. Rev. 43 (2014) 5896–5912.
- [40] Y. Kobayashi, B. Jacobs, M.D. Allendorf, J.R. Long, Chem. Mater. 22 (2010) 4120–4122.
- [41] M.A. Nasalevich, M.G. Goesten, T.J. Savenije, F. Kapteijn, J. Gascon, Chem. Commun. 49 (2013) 10575–10577.
- [42] P. Mahata, G. Madras, S. Natarajan, J. Phys. Chem. B 110 (2006) 13759–13768.
- [43] H. Li, M. Eddaoudi, M. O’Keeffe, O.M. Yaghi, Nature 402 (1999) 276–279.
- [44] M. Alvaro, E. Carbonell, B. Ferrer, F. Xamena, H. Garcia, Chem. – Eur. J. 13 (2007) 5106–5112.
- [45] L.M. Yang, G.Y. Fang, J. Ma, E. Ganz, S.S. Han, Cryst. Growth Des. 14 (2014) 2532–2541.
- [46] C.H. Hendon, D. Tiana, M. Fontecave, C. Sanchez, L. D’Arras, C. Sasse, L. Rozes, C. Mellot-Draznieks, A. Walsh, J. Am. Chem. Soc. 135 (2013) 10942–10945.
- [47] A. Dhakshinamoorthy, A.M. Asiri, H. Garcia, Angew. Chem. Int. Ed. 55 (2016) 5414–5445.
- [48] Y.H. Fu, D.R. Sun, Y.J. Chen, R.K. Huang, Z.X. Ding, X.Z. Fu, Z.H. Li, Angew. Chem. Int. Ed. 51 (2012) 3364–3367.
- [49] Y. Kataoka, K. Sato, Y. Miyazaki, K. Masuda, H. Tanaka, S. Naito, W. Mori, Energy Environ. Sci. 2 (2009) 397–400.
- [50] C.G. Silva, I. Luz, F. Xamena, A. Corma, H. Garcia, Chem. – Eur. J. 16 (2010) 11133–11138.
- [51] S. Okada, S. Ikurumi, T. Kamegawa, K. Mori, H. Yamashita, J. Phys. Chem. C 116 (2012) 14360–14367.
- [52] T. Kamegawa, Y. Masuda, N. Suzuki, Y. Horiuchi, H. Yamashita, ACS Appl. Mater. Interfaces 3 (2011) 4561–4565.
- [53] X.F. Qian, K. Fukui, Y. Kuwahara, T. Kamegawa, K. Mori, H. Yamashita, ChemSusChem 7 (2014) 1528–1536.
- [54] M. Dan-Hardi, C. Serre, T. Frot, L. Rozes, G. Maurin, C. Sanchez, G. Ferey, J. Am. Chem. Soc. 131 (2009) 10857–10859.
- [55] Y. Horiuchi, T. Toyao, M. Saito, K. Mochizuki, M. Iwata, H. Higashimura, M. Anjo, M. Matsuoka, J. Phys. Chem. C 116 (2012) 20848–20853.
- [56] L.J. Shen, M.B. Luo, L.J. Huang, P.Y. Feng, L. Wu, Inorg. Chem. 54 (2015) 1191–1193.
- [57] K. Mori, T. Itoh, H. Kakudo, T. Iwamoto, Y. Masui, M. Onaka, H. Yamashita, Phys. Chem. Chem. Phys. 17 (2015) 24086–24091.
- [58] K. Mori, H. Kakudo, H. Yamashita, ACS Catal. 4 (2014) 4129–4135.
- [59] X.J. Sun, Q. Yu, F.M. Zhang, J.Z. Wei, P. Yang, Catal. Sci. Technol. 6 (2016) 3840–3844.
- [60] X.Y. Dong, M. Zhang, R.B. Pei, Q. Wang, D.H. Wei, S.Q. Zang, Y.T. Fan, T.C.W. Mak, Angew. Chem. Int. Ed. 55 (2016) 2073–2077.
- [61] C.K. Prier, D.A. Rankic, D.W.C. MacMillan, Chem. Rev. 113 (2013) 5322–5363.
- [62] M. Zhu, Z. Li, Y. Du, Z. Mou, P. Yang, ChemCatChem 4 (2012) 112–117.
- [63] K. Mori, J. Aoyama, M. Kawashima, H. Yamashita, Dalton Trans. 43 (2014) 10541–10547.
- [64] A.J. Esswein, D.G. Nocera, Chem. Rev. 107 (2007) 4022–4047.
- [65] M.C. Wen, K. Mori, Y. Kuwahara, H. Yamashita, ChemCatChem 7 (2015) 3519–3525.
- [66] M. Zhu, Y. Dong, Y. Du, Z. Mou, J. Liu, P. Yang, X. Wang, J. Chem. Eur. 18 (2012) 4367–4374.
- [67] C. Wang, Z.G. Xie, K.E. deKrafft, W.L. Lin, J. Am. Chem. Soc. 133 (2011) 13445–13454.
- [68] Z.C. Wang, C.J. Medforth, J.A. Shelnutt, J. Am. Chem. Soc. 126 (2004) 16720–16721.
- [69] P.P. Guo, P.L. Chen, M.H. Liu, ACS Appl. Mater. Interfaces 5 (2013) 5336–5345.
- [70] I. Hod, M.D. Sampson, P. Deria, C.P. Kubiak, O.K. Farha, J.T. Hupp, ACS Catal. 5 (2015) 6302–6309.
- [71] A. Fateeva, P.A. Chater, C.P. Ireland, A.A. Tahir, Y.Z. Khimyak, P.V. Wiper, J.R. Darwent, M.J. Rosseinsky, Angew. Chem. Int. Ed. 51 (2012) 7440–7444.
- [72] J. Zheng, M.Y. Wu, F.L. Jiang, W.P. Su, M.C. Hong, Chem. Sci. 6 (2015) 3466–3470.
- [73] K. Sasan, Q.P. Lin, C.Y. Mao, P.Y. Feng, Chem. Commun. 50 (2014) 10390–10393.
- [74] S.C. Yu, S.J. Hou, W.K. Chan, Macromolecules 33 (2000) 3259–3273.
- [75] M.H. Zeng, X.L. Feng, X.M. Chen, Dalton Trans. (2004) 2217–2223.
- [76] E.D. Bloch, D. Britt, C. Lee, C.J. Doonan, F.J. Uribe-Romo, H. Furukawa, J.R. Long, O.M. Yaghi, J. Am. Chem. Soc. 132 (2010) 14382–14384.
- [77] T.H. Zhou, Y.H. Du, A. Borgna, J.D. Hong, Y.B. Wang, J.Y. Han, W. Zhang, R. Xu, Energy Environ. Sci. 6 (2013) 3229–3234.
- [78] C. Wang, K.E. deKrafft, W.B. Lin, J. Am. Chem. Soc. 134 (2012) 7211–7214.
- [79] M. Toyao, S. Saito, K. Dohshi, M. Mochizuki, H. Iwata, Y. Higashimura, M. Horiuchi, Matsuoka, Chem. Commun. 50 (2014) 6779–6781.
- [80] C.C. Hou, T.T. Li, S. Cao, Y. Chen, W.F. Fu, J. Mater. Chem. A 3 (2015) 10386–10394.
- [81] S. Pullen, H.H. Fei, A. Orthaber, S.M. Cohen, S. Ott, J. Am. Chem. Soc. 135 (2013) 16997–17003.
- [82] M.A. Nasalevich, R. Becker, E.V. Ramos-Fernandez, S. Castellanos, S.L. Veber, M.V. Fedin, F. Kapteijn, J.N.H. Reek, J.L. van der Vlugt, J. Gascon, Energy Environ. Sci. 8 (2015) 364–375.
- [83] Z. Yue, A. Liu, C. Zhang, J. Huang, M. Zhu, Y. Du, P. Yang, Appl. Catal. B 201 (2017) 202–210.
- [84] W.S. Xiaoping Chen, Front. Energy 7 (2013) 111–118.
- [85] K. Chang, X. Hai, J. Ye, Adv. Energy Mater. 6 (2016) 1502555.
- [86] Y.J. Wang, Y.N. Zhang, Z.Q. Jiang, G.Y. Jiang, Z. Zhao, Q.H. Wu, Y. Liu, Q. Xu, A.J. Duan, C.M. Xu, Appl. Catal. B 185 (2016) 307–314.
- [87] R. Lin, L.J. Shen, Z.Y. Ren, W.M. Wu, Y.X. Tan, H.R. Fu, J. Zhang, L. Wu, Chem. Commun. 50 (2014) 8533–8535.
- [88] J.J. Zhou, R. Wang, X.L. Liu, F.M. Peng, C.H. Li, F. Teng, Y.P. Yuan, Appl. Surf. Sci. 346 (2015) 278–283.
- [89] L.J. Shen, M.B. Luo, Y.H. Liu, R.W. Liang, F.F. Jing, L. Wu, Appl. Catal. B 166 (2015) 445–453.
- [90] J. He, Z.Y. Yan, J.Q. Wang, J. Xie, L. Jiang, Y.M. Shi, F.G. Yuan, F. Yu, Y.J. Sun, Chem. Commun. 49 (2013) 6761–6763.
- [91] C.W. Zhao, Y.A. Li, X.R. Wang, G.J. Chen, Q.K. Liu, J.P. Ma, Y.B. Dong, Chem. Commun. 51 (2015) 15906–15909.
- [92] R. Wang, L.N. Gu, J.J. Zhou, X.L. Liu, F. Teng, C.H. Li, Y.H. Shen, Y.P. Yuan, Adv. Mater. Interfaces 2 (2015) 1500037.
- [93] S. Saha, G. Das, J. Thote, R. Banerjee, J. Am. Chem. Soc. 136 (2014) 14845–14851.
- [94] Z.C. Lian, P.P. Xu, W.C. Wang, D.Q. Zhang, S.N. Xiao, X. Li, G.S. Li, ACS Appl. Mater. Interfaces 7 (2015) 4533–4540.
- [95] Q.Z. Wang, J.H. Lian, J.J. Li, R.F. Wang, H.H. Huang, B.T. Su, Z.Q. Lei, Sci. Rep. 5 (2015) 13593.
- [96] B. Cecconi, N. Manfredi, R. Ruffo, T. Montini, I. Romero-Ocana, P. Fornasiero, A. Abbotto, ChemSusChem 8 (2015) 4216–4228.
- [97] C.N.R. Rao, S.R. Lingampalli, Small 12 (2016) 16–23.
- [98] M.C. Yin, S. Ma, C.J. Wu, Y.T. Fan, RSC Adv. 5 (2015) 1852–1858.
- [99] P. Zhang, M. Wang, J.F. Dong, X.Q. Li, F. Wang, L.Z. Wu, L.C. Sun, J. Phys. Chem. B 114 (2010) 15868–15874.
- [100] T.T. Le, M.S. Akhtar, D.M. Park, J.C. Lee, O.B. Yang, Appl. Catal. B 111 (2012) 397–401.
- [101] X. Zong, Z. Xing, H. Yu, Y. Bai, G.Q. Lu, L.Z. Wang, J. Catal. 310 (2014) 51–56.
- [102] T. Kamegawa, S. Matsuura, H. Seto, H. Yamashita, Angew. Chem. Int. Ed. 52 (2013) 916–919.
- [103] B. Xiao, M. Zhu, X. Li, P. Yang, L. Qiu, C. Lu, Int. J. Hydrogen Energy 41 (2016) 11537–11546.
- [104] X. Liu, Y.X. Li, S.Q. Peng, H. Lai, Acta Phys.-Chim. Sin. 31 (2015) 612–626.
- [105] M.C. Wen, K. Mori, T. Kamegawa, H. Yamashita, Chem. Commun. 50 (2014) 11645–11648.
- [106] J. He, J.Q. Wang, Y.J. Chen, J.P. Zhang, D.L. Duan, Y. Wang, Z.Y. Yan, Chem. Commun. 50 (2014) 7063–7066.
- [107] R.W. Xin-Ling Liu, Ming-Yi Zhang, Yu-Peng Yuan, Can Xue, APL Mater. 3 (2015) 104403.
- [108] Y.P. Yuan, L.S. Yin, S.W. Cao, G.S. Xu, C.H. Li, C. Xue, Appl. Catal. B 168 (2015) 572–576.
- [109] W. Zhen, J. Ma, G. Lu, Appl. Catal. B 190 (2016) 12–15.
- [110] W.L. Zhen, H.B. Gao, B. Tian, J.T. Ma, G.X. Lu, ACS Appl. Mater. Interfaces 8 (2016) 10808–10819.
- [111] H.L. Wang, L.S. Zhang, Z.G. Chen, J.Q. Hu, S.J. Li, Z.H. Wang, J.S. Liu, X.C. Wang, Chem. Soc. Rev. 43 (2014) 5234–5244.
- [112] K.E. deKrafft, C. Wang, W.B. Lin, Adv. Mater. 24 (2012) 2014–2018.
- [113] M.H. Pham, C.T. Dinh, G.T. Vuong, N.D. Ta, T.O. Do, Phys. Chem. Chem. Phys. 16 (2014) 5937–5941.
- [114] I. Mondal, U. Pal, Phys. Chem. Chem. Phys. 18 (2016) 4780–4788.
- [115] S. Bala, I. Mondal, A. Goswami, U. Pal, R. Mondal, J. Mater. Chem. A 3 (2015) 20288–20296.
- [116] Y. Hou, J.Y. Li, Z.H. Wen, S.M. Cui, C. Yuan, J.H. Chen, Nano Energy 12 (2015) 1–8.
- [117] B. You, N. Jiang, M.L. Sheng, S. Gul, J. Yano, Y.J. Sun, Chem. Mater. 27 (2015) 7636–7642.
- [118] L. Jiao, Y.X. Zhou, H.L. Jiang, Chem. Sci. 7 (2016) 1690–1695.
- [119] K. Mori, K. Miyawaki, H. Yamashita, ACS Catal. 6 (2016) 3128–3135.
- [120] P. Verma, Y. Kuwahara, K. Mori, H. Yamashita, J. Mater. Chem. A 4 (2016) 10142–10150.
- [121] K. Mori, M. Dojo, H. Yamashita, ACS Catal. 3 (2013) 1114–1119.
- [122] A. Aijaz, T. Akita, N. Tsumori, Q. Xu, J. Am. Chem. Soc. 135 (2013) 16356–16359.
- [123] Q.L. Zhu, J. Li, Q. Xu, J. Am. Chem. Soc. 135 (2013) 10210–10213.
- [124] M.C. Wen, Y. Kuwahara, K. Mori, H. Yamashita, Top. Catal. 59 (2016) 1765–1771.
- [125] Y. Li, H. Xu, S.X. Ouyang, J.H. Ye, Phys. Chem. Chem. Phys. 18 (2016) 7563–7572.
- [126] M.C. Wen, Y. Kuwahara, K. Mori, D.Q. Zhang, H.X. Li, H. Yamashita, J. Mater. Chem. A 3 (2015) 14134–14141.
- [127] M.C. Wen, K. Mori, Y. Kuwahara, H. Yamashita, ACS Energy Lett. 2 (2017) 1–7.
- [128] M.C. Wen, Y.W. Cui, Y. Kuwahara, K. Mori, H. Yamashita, ACS Appl. Mater. Interfaces 8 (2016) 21278–21284.